Table 1. continued

gene ID	symbol	description	refs
51061	TXNDC11	thioredoxin domain containing 11	22
53347	UBASH3A	ubiquitin associated and SH3 domain containing A	22
10869	USP19	ubiquitin specific peptidase 19	22
9218	VAPA	VAMP (vesicle-associated membrane protein)-associated protein A, 33 kDa	22
9217	VAPB	VAMP (vesicle-associated membrane protein)-associated protein B and C	this study; 22,28,46
10493	VAT1	vesicle amine transport protein 1 homologue (*T. californica*)	this study
55737	VPS35	vacuolar protein sorting 35 homologue (*S. cerevisiae*)	22
6293	VPS52	vacuolar protein sorting 52 homologue (*S. cerevisiae*)	22
140612	ZFP28	zinc finger protein 28 homologue (mouse)	this study
9726	ZNF646	zinc finger protein 646	22

Quantitative Reverse-Transcription PCR (qRT-PCR)

Total RNA was prepared from the cell and culture supernatant using the RNeasy mini kit (QIAGEN, Hilden, Germany) and QIAamp Viral RNA Mini Kit (QIAGEN), respectively. First-strand cDNA was synthesized using high capacity cDNA reverse transcription kit (Applied biosystems, Carlsbad, CA, USA) with random primers. Each cDNA was estimated by Platinum SYBR Green qPCR Super Mix UDG (Invitrogen) as per the manufacturer's protocol. Fluorescent signals of SYBR Green were analyzed with ABI PRISM 7000 (Applied Biosystems). The HCV internal ribosomal entry site (IRES) region and human glyceraldehyde-3-phosphate dehydrogenase (GAPDH) gene were amplified with the primer pairs 5′-GAGTGTCGTGCAGCCTCCA-3′ and 5′-CACTCG-CAAGCACCCTATCA-3′, and 5′-GAAGGTCGGAGT-CAACGGATT-3′ and 5′-GATGACAAGCTTCCCGTTCTC-3′, respectively.[42] The quantities of the HCV genome and the other host mRNAs were normalized with that of GAPDH mRNA. RTN1 and RTN3 genes were amplified using the primer pairs purchased from QIAGEN.

Cell Lines and Virus Infection

Cells from the Huh7OK1 cell line are highly permissive to HCV JFH1 strain (genotype 2a) infection compared to Huh 7.5.1 and exhibit the highest propagation efficiency for JFH1.[43] These cells were maintained at 37 °C in a humidified atmosphere and 5% CO_2, in the Dulbecco's modified Eagle's medium (DMEM) (Sigma, St. Louis, MO, USA) supplemented with nonessential amino acids (NEAA) and 10% fetal calf serum (FCS). The viral RNA of JFH1 was introduced into Huh7OK1 as described by Wakita et al.[44] The viral RNA of JFH1 derived from the plasmid pJFH1 was prepared as described by Wakita et al.[44]

Statistical Analysis

Experiments for RNAi transfection and qRT-PCR were performed two times. The estimated values were represented as the mean ± standard deviation (n = 2). The significance of differences in the means was determined by the Student's t-test.

RESULTS AND DISCUSSION

Identifying Host Proteins That Interact with HCV NS5A Protein

We employed an integrated approach that combined an experimental Y2H assay and comprehensive literature mining to identify human host proteins interacting with NS5A.

First, we performed an Y2H screening to characterize the interactions between NS5A and host proteins. The analysis of positive colonies revealed 17 host factors as interacting partners of NS5A (Tables 1, S1, Supporting Information), 14 of which are novel. The other three interactions have been characterized previously; vesicle-associated membrane protein (VAMP)-associated protein B (VAPB), a membrane trafficking factor, and FK506-binding protein 8 (FKBP8), an immunoregulation protein, independently regulate HCV replication via interactions with NS5A;[28,43,45,46] Bridging integrator 1 (BIN1), a tumor suppressor protein, interacts with NS5A and significantly contributes to HCC.[47] Among the newly discovered interactors, MAP4K4 is overexpressed in HCC, and knockdown of MAP4K4 expression inhibits HCC progression;[48] RTN1 and VAT1 were previously observed to be elevated in HCV infected cells,[49] and ARL6IP1, EPHB6, GABARAPL2, ITSN1 and NISCH were differentially expressed in HCV infection in vitro.[50] Furthermore, five (ARL6IP1, FKBP8, RTN1, RTN3, VAPB) of the 17 interactors (29.4%) localize to the endoplasmic reticulum (ER; GO:0005783; p = 0.0028), which is consistent with the role of NS5A as a crucial constituent of the HCV replication complex associated with the ER.[51] These results suggest that the PPIs detected by our Y2H assay may closely reflect NS5A interactions in vivo.

We next scanned the biomedical literature to expand the repertoire of NS5A–host interactions. Because of an ever increasing volume of biomedical literature describing the pathogenesis of infectious diseases, the identification of specific host–pathogen interactions and their roles in pathogenicity is a nontrivial task, and therefore, recent years have witnessed a rapid development of computational tools for biomedical literature mining. We performed extensive literature mining using computational tools that facilitate the retrieval and extraction of relevant information from the biomedical literature (Pubmed, EBIMed, Protein Coral) and followed it up with a careful manual inspection to identify additional host factors, which directly interact with NS5A and which were not present in the Y2H data set. One hundred and fifteen pairwise interactions between NS5A and human proteins (consisting of 93 catalogued by a high throughput study of binary HCV–host interactions[22] and 22 from assorted reports; see Supporting Information, Table S2) were extracted from the literature in this manner and were added to the existing interactors. The resulting NS5A–human interactome thus comprised 132 human host proteins directly interacting with NS5A (Table 1), all of which are expressed in the liver (see Supporting Information, Table S3).

Network Topological Analysis of the NS5A–host Interactions: NS5A Preferentially Targets Hubs and Bottlenecks in the Host Protein Interactome

To further understand the biological significance of the NS5A–host interactions, we retrieved PPIs for the nodes targeted by

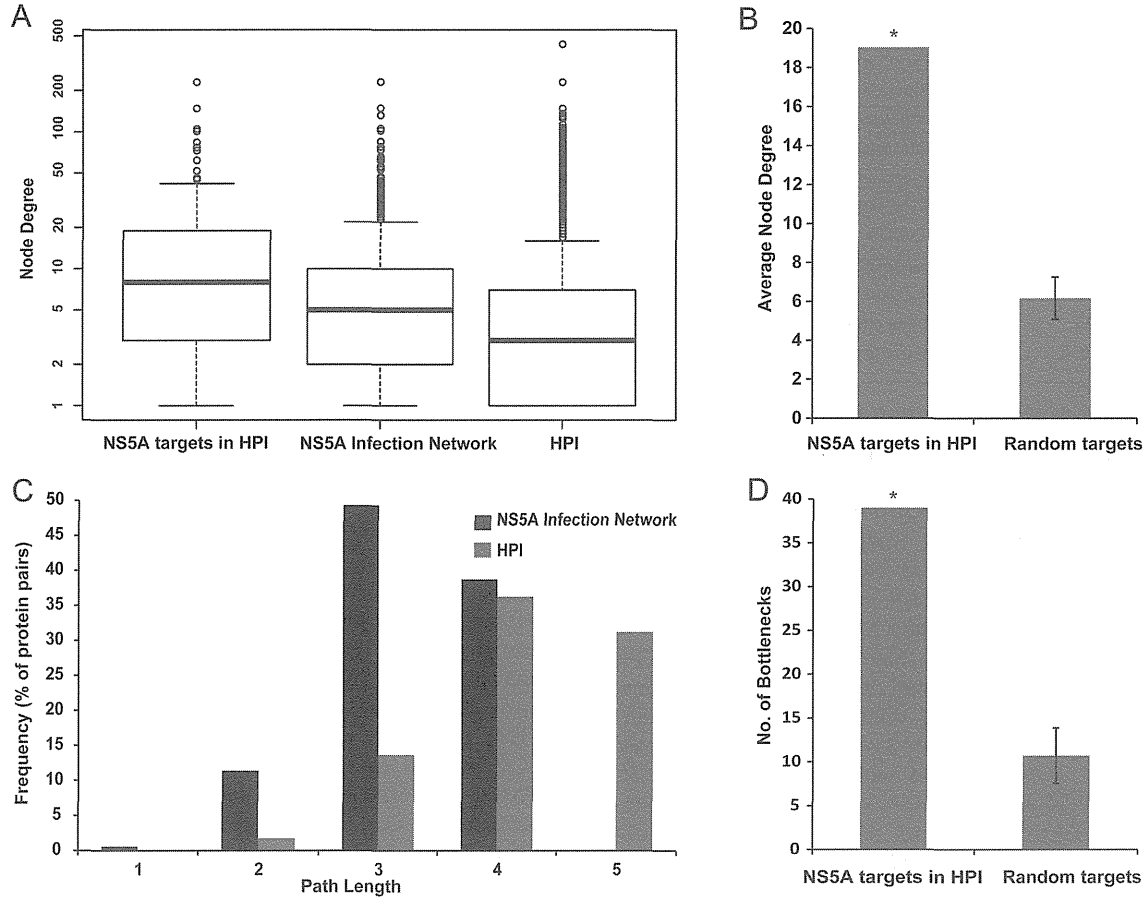

Figure 1. Topological analysis of the NS5A infection network. (A) The node degree distributions of the NS5A interatcors in the HPI, NS5A infection network, and HPI are represented as box plots. The average degree of the NS5A interactors in HPI (19.02) was higher than those of the NS5A infection network (8.24) and HPI (5.96). Median node degrees (indicated by thick horizontal lines) of the NS5A interactors in HPI, NS5A infection network, and HPI are 8, 5, and 3, respectively. (B) The average degree of the nodes targeted by NS5A in HPI was much higher than mean average degree of 1000 sets of the randomly selected 108 nodes in HPI. (C) The shortest path length distributions of the NS5A infection network and HPI. The path length is represented on the *x*-axis while the *y*-axis describes the frequency, i.e., the percentage of node (protein) pairs within the PPI network with a given shortest path length. For simplicity, only the node frequencies for path lengths 1−5 in the HPI are displayed. (D) The number of bottlenecks among the nodes targeted by NS5A in HPI was much higher than mean of the number of bottlenecks among 1000 sets of the randomly selected 108 nodes in HPI. *: $p < 0.001$.

NS5A in the HPI and incorporated them with the initial interactions to infer an extended NS5A infection network. PPIs for 108 of 132 NS5A interactors were retrieved in this manner; 24 of 132 NS5A interactors had no PPIs in the HPI (Supporting Information, Tables S4, S5a, S5b). For the NS5A infection network and the HPI, we computed the node degree distribution and the characteristic/average path length measures to capture the topologies of the two networks. The degree of a protein, which corresponds to the number of its interacting partners, may often reflect its biological relevance since a better connected protein is likely to have a higher ability to influence biological networks via PPIs. Average path lengths provide an approximate measure of the relative ease and speed of dissemination of information between the proteins in a network.

The NS5A infection network consisted of 1442 entities (nearly all of which are expressed in the liver; see Supporting Information) with 6263 interactions between them (Supporting Information, Tables S4, S5a). The average degree (defined as the number of interactions for a given protein) of the NS5A infection network (8.24) was notably higher than the degree inferred for the HPI (5.96) (Figure 1A). Furthermore, the average degree of the nodes targeted by NS5A in the HPI (19.02) was even higher; this number is significantly greater than the average degree obtained from a sample of randomly selected nodes (6.17 ± 1.08 with $p < 0.001$; Figure 1B; see Supporting Information). Also the degrees inferred for the majority of the NS5A interactors in the HPI (65 of 108; 60.18%) were higher than the mean degree of the HPI (5.96) (Figure 1A). Our observations therefore suggest that NS5A preferentially targets several highly connected cellular proteins (hubs) with an ability to influence a large number of host factors in HCV infection. The average (shortest) path length of the NS5A infection network (3.26) was significantly shorter than the HPI (4.54), and also the distribution of shortest path lengths was shifted toward the left (Figure 1C), thereby suggesting that the NS5A influenced cellular network is more compact and inclined toward faster communication between the constituents relative to the host cellular network.

Next, we examined the betweenness measures of the NS5A interactors in the HPI to assess their significance in the HPI and the NS5A infection network. The betweenness of a node, determined by the number of shortest paths passing through it, reflects the importance of that node in the network; the nodes

with the highest betweenness prominently regulate the flow of signaling information and are therefore "bottlenecks", representing central points for communication in an interaction network.[52] Previously, proteins with high betweenness have been implicated in crucial roles in HCV infection and pathogenesis.[53,54] To investigate if NS5A preferentially targets bottlenecks (defined as the top 10% of the nodes in the HPI ranked by betweenness), we estimated the fraction of NS5A interactors that were bottlenecks in the HPI. A significant proportion (39 of 108; 36.1%) of the NS5A interactors were identified as bottlenecks in the HPI (Supporting Information, Table S6); this number is significantly higher than the number of bottlenecks among randomly selected nodes (10.72 ± 3.17 with $p < 0.001$; Figure 1D; see Supporting Information). These include growth factor receptor-binding protein 2 (GRB2), which plays an important role in the subversion of host signaling pathways by NS5A;[55] tumor protein 53 (TP53), a key mediator of the oncogenic effect of NS5A in HCV-induced HCC;[56] and tyrosine kinase SRC, which regulates the formation of NS5A-containing HCV replication complex.[57] Among the NS5A interacting proteins identified by our Y2H screening, ITSN1, an endocytic traffic associated protein, and GABARAPL2, an autophagy associated protein, were identified as network bottlenecks.

Our observations therefore suggest that NS5A preferentially interacts with highly central proteins in the host protein interactome; these interactions may help the virus to regulate efficiently the flow of the infection-related information in the host cellular network and manipulate the host metabolic machinery for its own survival and pathogenesis. Our observations are consistent with studies that suggested that viral pathogens tend to interact with well-connected host proteins that are central to the host cellular networks, thus enabling them to appropriate essential cellular functions.[21,22,26,58,59]

Functional Analysis of NS5A Interaction Network

Next, we investigated the NS5A infection network for the enrichment of specific biological associations (KEGG pathways, CATH structural domains; GO terms and Reactome Pathways; Supporting Information, Tables S7a, S7b, S7c and S7d). Notably, a significant proportion of the proteins in the NS5A infection network were mapped to the CATH Phosphorylase Kinase; domain 1, domain (CATH:3.30.200.20; 138 out of 1442, $p = 2.61 \times 10^{-45}$) including 23 of the 132 NS5A interacting host proteins ($p = 3.38 \times 10^{-14}$) (13 of which are bottlenecks in the HPI), based on the Gene3D protein domain assignments (Supporting Information, Table S7b). These include two novel interactions between EPHB6 (a kinase deficient receptor) and MAP4K4 and NS5A, identified by our Y2H assay (Table 1). The significant representation of cellular kinases in the NS5A infection network is consistent with the key roles played by reversible phosphorylation of NS5A in modulating various NS5A functions in HCV pathogenesis. Impairing NS5A hyperphosphorylation has been shown to inhibit HCV replication, and thus, the cellular kinases that regulate NS5A phosphorylation are important targets for anti-HCV therapy.[9,60−63]

The analysis of NS5A infection network revealed an enrichment of 79 KEGG pathways (Supporting Information, Table S7a). Furthermore, 31 of the 39 NS5A interacting bottlenecks (hereafter referred to as bottlenecks) were mapped to 75 of the 79 enriched KEGG pathways (Supporting Information, Table S5). Among the 75 bottleneck-associated enriched KEGG pathways, the highest numbers were associated with various cancers and infectious diseases (31 enriched KEGG pathways; 27 bottlenecks), followed by immune system, signal transduction and endocrine system (23 enriched KEGG pathways; 27 bottlenecks), cell growth and death (4 enriched KEGG pathways; 9 bottlenecks), nervous system (4 enriched KEGG pathways; 8 bottlenecks) and cellular communication (3 enriched KEGG pathways; 14 bottlenecks) among others (Tables 2, S8a, Supporting Information). Below we describe our observations on the most prominent enriched biological themes of interest that were associated with the NS5A infection network, with a specific focus on the bottlenecks.

Cancers and Infectious Diseases

The analysis of the NS5A interaction network revealed that NS5A specifically targets host factors that participate in various complex human diseases. Thirty-four NS5A interactors including 24 bottlenecks were mapped to one or more of the 17 enriched KEGG pathways associated with different infectious diseases (Supporting Information, Tables S7a, S8a). Among the most prominent associations, 12 bottlenecks were mapped to "Epstein−Barr virus infection" ($p = 1.36 \times 10^{-27}$); 10 to "Hepatitis C" ($p = 3.47 \times 10^{-24}$); 10 to "HTLV-I infection" ($p = 1.39 \times 10^{-20}$); 9 to "Hepatitis B" ($p = 3.33 \times 10^{-26}$); 8 to "Measles" ($p = 5.69 \times 10^{-17}$); 7 bottlenecks were mapped to "Influenza A" ($p = 5.01 \times 10^{-12}$); 7 to "Herpes simplex infection" ($p = 1.47 \times 10^{-13}$) and 6 to "Tuberculosis" ($p = 3.02 \times 10^{-6}$) (Supporting Information, Tables S7a, S8a). These associations include infectious diseases induced by various bacterial and viral pathogens thereby suggesting that HCV and other pathogens may systematically target specific host factors, the perturbation of which may contribute to the onset of various human diseases.

Also, 19 bottlenecks were mapped to one or more of the 16 enriched KEGG pathways associated with various cancers. Among the most prominent associations, 10 bottlenecks were mapped to "Viral carcinogenesis" ($p = 1.3 \times 10^{-30}$); 8 each were mapped to "Prostrate cancer" ($p = 4.27 \times 10^{-25}$), "Endometrial cancer" ($p = 5.52 \times 10^{-21}$) and "Colorectal cancer" ($p = 4.22 \times 10^{-18}$); 7 to "Pancreatic cancer" ($p = 1.94 \times 10^{-18}$); 6 to "Chronic myeloid leukemia" ($p = 1.61 \times 10^{-30}$) and 5 each to "Non-small cell lung cancer" ($p = 8.66 \times 10^{-15}$) and "Glioma" ($p = 2.38 \times 10^{-14}$) (Supporting Information, Tables S7a, S8a). The significant association of HCV with host factors central to various cancer pathways (including tumor suppressors such as TP53) is consistent with previous observations that viral pathogens significantly targeted host proteins associated with cancer pathways,[59,64,65] which likely plays major roles in tumorigenesis.

Immune System and Signal Transduction

HCV infection induces various active and passive host immune responses including the recognition of viral RNA by host cell receptors. These events lead to the production of Type I interferons (IFN-α/β) and inflammatory cytokines in the infected hepatocytes, initiating the antiviral response. HCV persistence in the host is determined by the virus's ability to impair host immune responses.[66−69]

The analysis of the NS5A interaction network revealed that 21 of the 132 NS5A interacting proteins, including 16 bottlenecks and their interacting partners, were mapped to one or more enriched KEGG pathways associated with the immune system (Supporting Information, Tables S7a, S8a).

Table 2. KEGG Pathway Functional Categories (Subclasses) Sorted by the Number of Enriched Pathways (≥3) Associated with One or More NS5A Interacting Bottlenecks

category	no. of enriched pathways	no. of bottlenecks	associated bottlenecks	KEGG pathways in the given category associated with most number of bottlenecks
infectious diseases	16	24	ACTB, AKT1, CDK1, CSNK2A1, CTNNB1, FLNA, FYN, GPS2, GRB2, GSK3B, HSPB1, JAK1, LCK, LYN, PIK3R1, PPP2CA, RAF1, SRC, STAT1, SYK, TBP, TGFBR1, TP53, TRAF2	"Epstein–Barr virus infection"; "HTLV-I infection"; "Hepatitis C"; "Hepatitis B"; "Measles"; "Influenza A"; "Herpes simplex infection"; "Tuberculosis"; "Toxoplasmosis"; "Chagas disease (American trypanosomiasis)"; "Bacterial invasion of epithelial cells"
cancers	16	19	AKT1, AXIN1, CDK1, CTNNB1, GRB2, GSK3B, HSP90AA1, JAK1, LYN, RAF1, SRC, STAT1, SYK, TBP, TGFBR1, THBS1, TP53, TRAF2	"Pathways in cancer"; "Viral carcinogenesis"; "Prostate cancer"; "Endometrial cancer"; "Colorectal cancer"; "Pancreatic cancer"; "Chronic myeloid leukemia"; "Non-small cell lung cancer"; "Glioma"; "Small cell lung cancer"; "Renal cell carcinoma"; "Melanoma"; "Acute myeloid leukemia"
immune system	10	16	ACTB, AKT1, CTNNB1, FYN, GRB2, GSK3B, HSP90AA1, LCK, LYN, PIK3R1, PIN1, RAF1, SRC, STAT1, SYK, TRAF	"Chemokine signaling pathway"; "T cell receptor signaling pathway"; "Fc epsilon RI signaling pathway"; "B cell receptor signaling pathway"; "Natural killer cell mediated cytotoxicity"; "Fc gamma R-mediated phagocytosis"
signal transduction	9	22	AKT1, AXIN1, CSKN1A1, CTNNB1, FLN, GRB2, GSK3B, HSP90AA1, HSPB1, JAK1, LCK, LYN, PIK3R1, PPP2CA, RAF1, SRC, STAT1, SYK, TGFBR1, THBS1, TP53, TRAF2	"PI3K-Akt signaling pathway"; "MAPK signaling pathway"; "Wnt signaling pathway"; "ErbB signaling pathway"; "VEGF signaling pathway"; "NF-kappa B signaling pathway"; "Jak-STAT signaling pathway"
nervous system	5	8	AKT1, GRB2, GSK3B, LYN, PIK3R1, PPP2CA, RAF1, TP53	"Neurotrophin signaling pathway"; "Long-term depression"; "Dopaminergic synapse"; "Long-term potentiation"
endocrine system	4	10	AKT1, CDK1, GRB2, GSK3B, HSP90AA1, PIK3R1, PLK1, RAF1, SRC, TRAF2	"Progesterone-mediated oocyte maturation"; "Insulin signaling pathway"; "GnRH signaling pathway"; "Adipocytokine signaling pathway"
cell growth and death	4	9	AKT1, CDK1, GSK3B, PIK3R1, PLK1, PPP2CA, THBS1, TP53, TRAF2	"Cell cycle"; "Apoptosis"; "p53 signaling pathway"; "Oocyte meiosis"
cell communication	3	14	ACTB, AKT1, CSNK2A1, CTNNB1, FLNA, FYN, GRB2, GSK3B, PIK3R1, PPP2CA, RAF1, SRC, TGFBR1, THBS1	"Focal adhesion"; "Tight junction"; "Adherens junction"
development	3	12	AKT1, FHL2, FYN, GRB2, GSK3B, JAK1, LCK, PIK3R1, STAT1, SYK, TGFBR1, THBS1	"Osteoclast differentiation"; "Axon guidance"; "Dorso-ventral axis formation"

Eight bottlenecks were mapped to the enriched KEGG pathway "Chemokine signaling pathway" ($p = 2.27 \times 10^{-10}$), which is consistent with the modulation of host interferon signaling by NS5A in HCV infection.[70] In addition, 7 bottlenecks each were mapped to "T cell receptor signaling pathway" ($p = 4.6 \times 10^{-24}$), "Fc epsilon RI signaling pathway" ($p = 2.86 \times 10^{-14}$) and "B cell receptor signaling pathway" ($p = 1.8 \times 10^{-14}$) and 6 bottlenecks were mapped to "Natural killer cell mediated cytotoxicity" ($p = 1.92 \times 10^{-12}$). Three bottlenecks (AKT1, PIK3R1 and STAT1) were also mapped to the enriched KEGG pathway "Toll-like receptor signaling pathway" ($p = 3.23 \times 10^{-7}$; Supporting Information, Tables S7a, S8a). Toll-like receptor 3 mediated chemokine and cytokine signaling plays an important role in the host immune response in HCV infection.[71] Therefore, NS5A interaction with bottlenecks, which function in various aspects of the host immune response, may significantly contribute to the perturbation of the host immune system in HCV pathogenesis.

Additionally, 32 of 132 NS5A interacting proteins examined in the present study, including 24 bottlenecks, were mapped to various pathways associated with the signal transduction and the endocrine system (Supporting Information, Tables S7a, S8a), many of which are implicated in HCV infection and HCC progression and are targets for molecular therapy in HCC.[22,72−74]

Eleven bottlenecks were mapped to the enriched KEGG pathway "PI3K-Akt signaling pathway" ($p = 2.2 \times 10^{-24}$; Supporting Information, Tables S7a, S8a), which is consistent with a previous study that NS5A stimulates the activation of PI3K-Akt pathway, which contributes to HCC in HCV infection.[75] Eight bottlenecks were mapped to the enriched KEGG pathway "MAPK signaling pathway" ($p = 2.4 \times 10^{-19}$; Supporting Information, Tables S7a, S8a). Elements of the MAPK signaling cascades are directly involved in the progression of HCV infection, particularly in association with HCV Core and E2 proteins,[22,24,76,77] thereby suggesting that NS5A interactions with the key facilitators of MAPK signaling in the host interactome may play an important role in regulating the reversible phosphorylation of NS5A and may contribute to the progression of HCV pathogenesis.

Bottlenecks AKT1, GRB2, GSK3B, PIK3R1 and RAF1 and many of their interactors were mapped to the enriched KEGG pathway "Insulin signaling pathway" ($p = 2.42 \times 10^{-13}$; Supporting Information, Tables S7a, S8a); these proteins are highlighted in Figure 2. Insulin signaling plays an important role in regulating glucose and lipid metabolism, and the disruption of this process may contribute to insulin resistance (IR). IR is linked with steatosis, fibrosis progression and poor interferon-α response in HCV infection.[78−80] Suppression of AKT1 and GSK3B activity in HCV infection disrupts glucose metabolism and contributes to IR.[81,82] Furthermore, PIK3R1 and NS5A interactor PIK3CB (Figure 2) are subunits of phosphatidylinositol 3-kinase (PI3K), which controls insulin secretion;[83] PI3K also facilitates the activation of the proto-oncogene beta-catenin (CTNNB1) by NS5A, which contributes to the development of HCC in HCV pathogenesis.[84] Previously, HCV Core protein has been directly implicated in the induction of IR in HCV infection,[85] while there is little evidence suggesting definitive links between NS5A and IR. Our observations, however, suggest that NS5A directly interacts with key regulators of insulin metabolism and may, therefore, play a major role in modulating HCV-induced IR and eventually HCC.

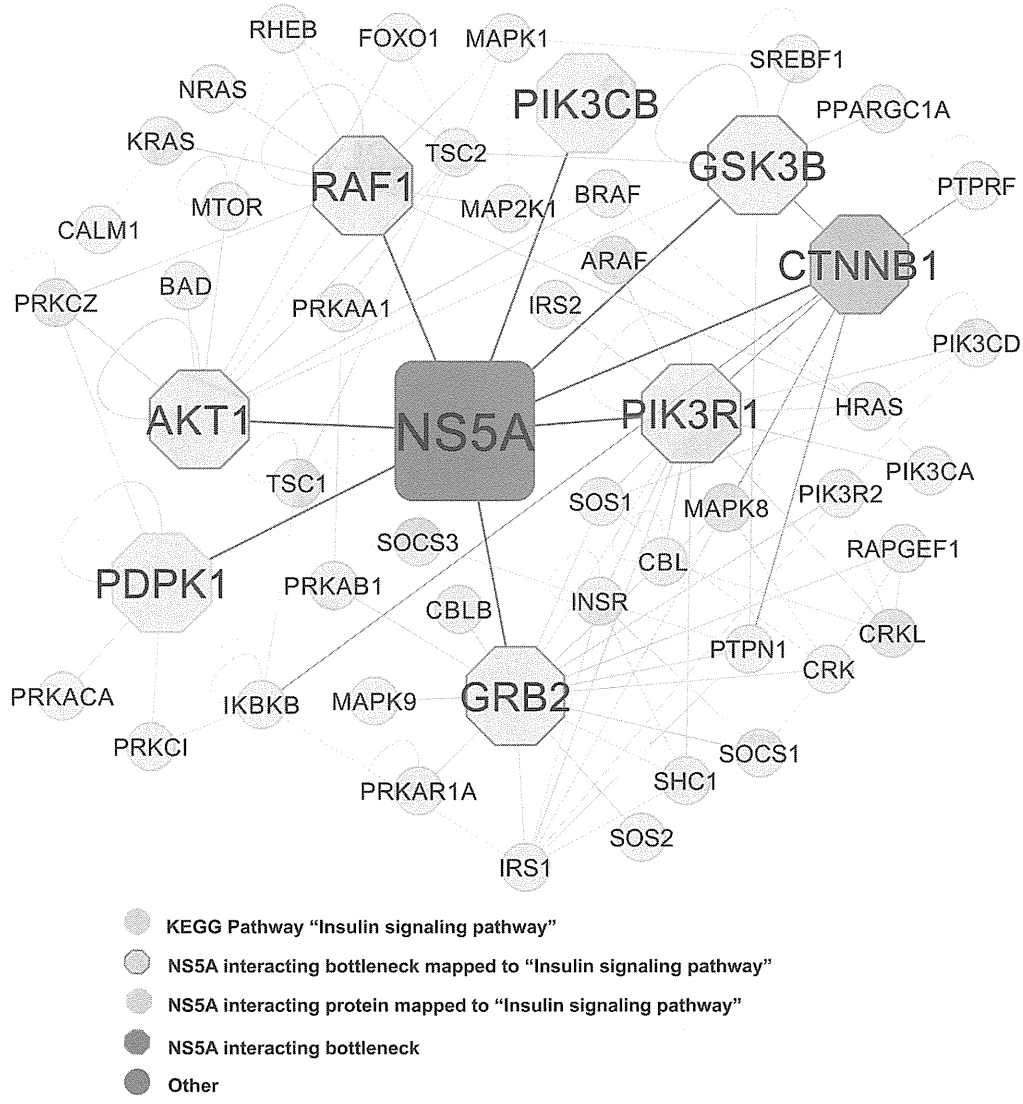

Figure 2. NS5A interacting bottlenecks and their interacting partners associated with the enriched KEGG pathway hsa04910: "Insulin signaling pathway".

Cell Adhesion and Communication

The perturbation of adherens and tight junction associated proteins has been implicated in HCV entry, cell–cell transmission and hepatoma migration in HCV infection.[86–88] In the NS5A infection network, eight bottlenecks (ACTB, AKT1, CSNK2A1, CTNNB1, FYN, PPP2CA, SRC and TGFBR1) were mapped to either or both of the enriched KEGG pathways "Adherens Junction" ($p = 1.03 \times 10^{-15}$) and "Tight junction" ($p = 1.19 \times 10^{-5}$), which are associated with cell adhesion junctions and cellular communication (Supporting Information, Tables S7a, S8a). CSNK2A1 is the catalytic (alpha) subunit of Casein Kinase II (CK2), which phosphorylates NS5A and regulates the production of infectious viral particles.[63] CTNNB1, a key component of cell-adhesion complexes, is positively regulated by CK2.[89] Furthermore, the activation of CTNNB1 by NS5A significantly contributes to HCC.[84] Taken together, our observations suggest that NS5A interactions with bottlenecks, which regulate cell–cell adhesion (CSNK2A1, CTNNB1) and cytoskeletal organization (ACTB), may significantly contribute to the progression of HCV life cycle and tumorigenesis in HCV pathogenesis.

Eleven bottlenecks were mapped to the enriched KEGG pathway "Focal Adhesion" ($p = 1.02 \times 10^{-17}$; Supporting Information, Tables S7a, S8a), thereby reiterating that focal adhesion is a major target of NS5A.[22] Focal adhesion regulates cell migration and adhesion, and some of its components were directly implicated in the regulation of HCV replication and propagation in our earlier study.[24] Our observations thus suggest that NS5A interactions with key components of the focal adhesion machinery may play important roles in the HCV lifecycle. For instance, NS5A interacts with bottleneck THBS1 (Thrombospondin-1), a glycoprotein, which was mapped to the KEGG "Focal Adhesion" pathway. THBS1 plays a key role in NS5A-mediated activation of the cytokine TGF-β1, which facilitates HCV replication and progressive liver fibrosis in HCV infection.[90] Our observations suggest that direct NS5A interactions with the bottlenecks THBS1 and TGFBR1 (TGF-β receptor 1; KEGG Pathway "Adherens Junction"), a key facilitator of TGF-β downstream signaling, may be crucial in facilitating HCV replication and tumorigenesis in HCV pathogenesis.

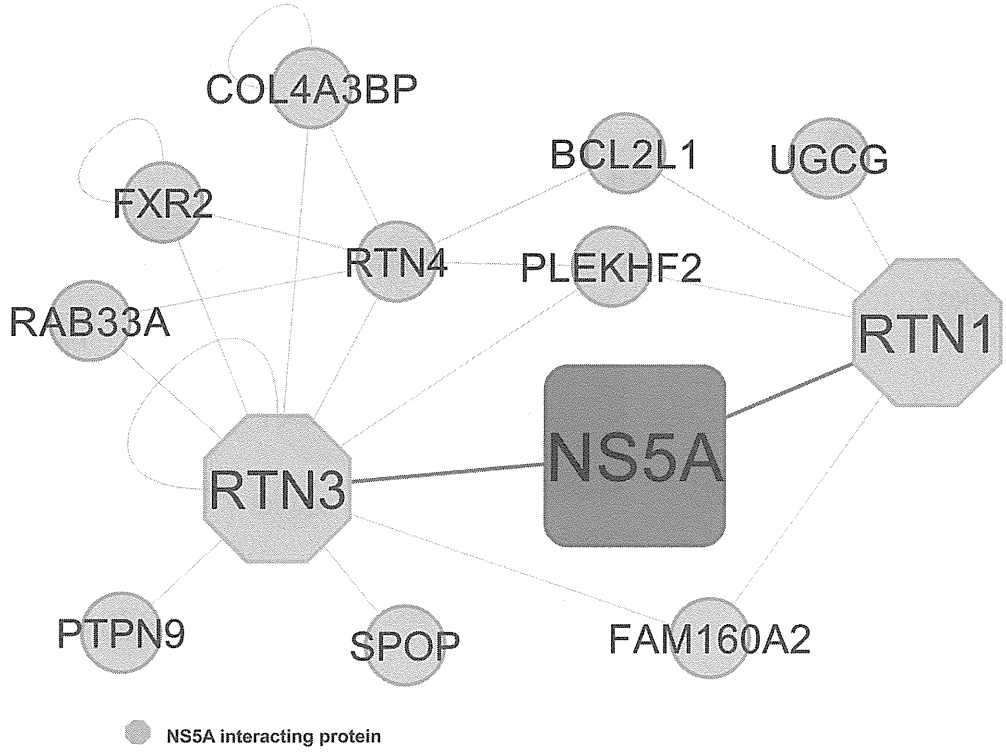

Figure 3. ER-localized host factors RTN1 and RTN3 were found to interact (blue edges) with NS5A in an Y2H screening of human liver cDNA library using NS5A as bait.

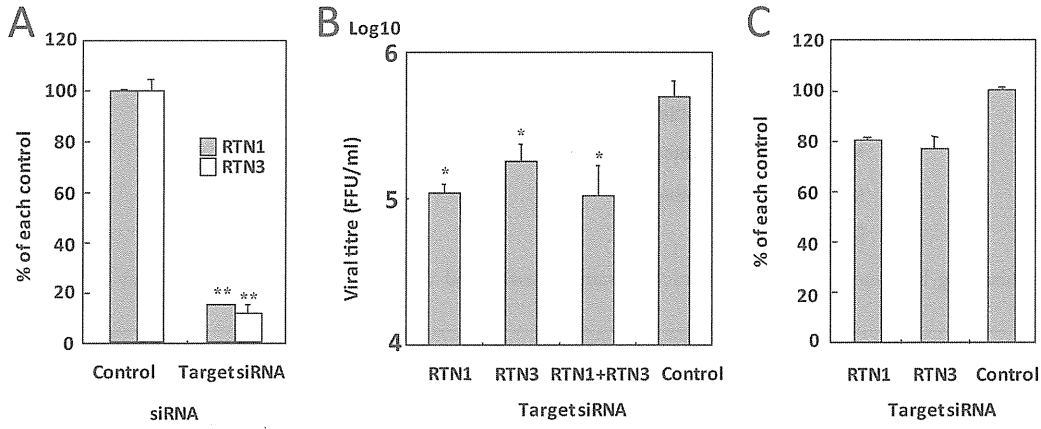

Figure 4. Effects of knockdown of RTN1 and RTN3 on HCV propagation and replication. Host factors RTN1 and RTN3 were suppressed by RNAi (A) in Huh7OK1 cells infected with HCV JFH1 strain (genotype 2a). The amounts of viral titer (B) and intracellular viral RNA (C) were estimated. Each value was represented as percentage of the cells transfected with the control siRNA. FFU: Focus-forming units; *: $p < 0.05$, **: $p < 0.01$.

Cellular Transport

Cellular factors associated with endocytic trafficking are key facilitators of the HCV life cycle, particularly HCV entry into the hepatic cells.[91−93] Endocytosis of the extracellular growth factor receptor (EGFR) in association with the cell surface glycoprotein CD81 plays a crucial role in HCV internalization and entry and is, therefore, an attractive target of anti-HCV strategies.[94] In the NS5A infection network, NS5A interactors ARAP1 and HSPA1A together with two bottlenecks (SRC, TGFBR1) were mapped to the enriched KEGG pathway "Endocytosis" ($p = 2.97 \times 10^{-8}$; Supporting Information, Tables S7a, S8a). ARAP1, a Golgi associated protein, negatively regulates EGFR trafficking, and decreased ARAP1 expression contributes to enhanced EGFR endocytosis.[95] Therefore, NS5A interaction with ARAP1 may facilitate EGFR internalization and thus viral entry in HCV infection.

NS5A Interacting Host Proteins RTN1 and RTN3 Function in HCV Propagation but Not Replication

Traditionally, viral and host proteins associated with the HCV lifecycle (internalization, replication, assembly and release) have been preferred targets in the anti-HCV studies. During infection, HCV localizes to the detergent-resistant membrane fraction (DRM) derived from the ER, where the viral replication and assembly take place.[4] Thus, of the novel interactions identified in our Y2H assay, we focused on two ER-localized host factors RTN1 and RTN3 (Figure 3). RTN1 and RTN3 belong to a group of proteins named Reticulons, which are integral to maintaining the shape and organization of the

ER and have been implicated in facilitating the replication of various positive-strand RNA viruses.[96−98] Furthermore, both RTN1 and RTN3 have been specifically detected in the very low density lipoprotein (VLDL) transport vesicle (VTV);[99] VTV is a key component of the VLDL secretory pathway, which plays an essential role in the production and the release of the infectious HCV particles.[100] Therefore, NS5A interactions with RTN1 and RTN3 suggested novel and potentially crucial roles of the two host proteins in the replication and/or release stages of the HCV lifecycle.

We performed cellular assays to assess the impact of RTN1 and RTN3 siRNA knockdowns on HCV replication and release. Since the HCV-production systems using the HCV JFH1 infectious strain (genotype 2a) isolates alone are capable of both efficient replication and the production of the infectious HCV particles, JFH1 was used to infect the Huh7OK1 cell line 24h after transfection with each siRNA (see Materials and Methods). The infected cells were harvested after 72 h postinfection, and the expression of each host protein was assessed by qRT-PCR (Figure 4A). The viral titer was significantly decreased by individual and double knockdowns of RTN1 and RTN3 (Figure 4B). However, RTN1 and RTN3 knockdowns had no effect on the intracellular viral RNA levels in the HCV infected cells (Figure 4C), suggesting that RTN1 and RTN3 regulate HCV propagation but not HCV replication.

CONCLUSIONS

We describe here our observations of PPIs between HCV NS5A and host proteins. By employing a multifold approach involving an experimental Y2H assay and literature mining, we derived a comprehensive set of experimentally determined binary interactions between NS5A and host proteins. We proceeded to map the combined NS5A−host interactions onto an overall interaction network, which comprised a repertoire of connections, which potentially enable NS5A to link up with and modulate the components of the host cellular networks. We then employed a network-based approach to understand the biological context of these connections in HCV pathogenesis with the help of the TargetMine data warehouse.

A functional analysis of the PPI networks highlighted NS5A interactions with several well connected host factors (hubs) and centrally located "bottlenecks" in the host cellular networks that function in cellular pathways associated with immune system and cell signaling, cellular adhesion and cell transport, cell growth and cell death and ER homeostasis among others. The "bottlenecks" include several proteins that were previously implicated in HCV pathogenesis, thereby suggesting that NS5A interactions with centrally connected host factors may enable the virus to influence strongly the host cellular processes in HCV infection. Notably, many bottlenecks were mapped to pathways associated with the infectious diseases induced by diverse bacterial and viral pathogens of the human host. These observations thus suggest the presence of some common themes underlying the onset of various human diseases associated with pathogenic infection in humans, a better understanding of which may be helpful in optimizing broad spectrum approaches to counteracting a wide range of pathogenic infections.

Cellular assays based on siRNA knockdowns in the HCV infected and replicon cells demonstrated RTN1 and RTN3, ER-localized NS5A interacting proteins, to be novel regulators of HCV propagation, but not replication, and thus promising novel candidates for anti-HCV therapy.

Our analysis therefore provides further insights into the role of NS5A−host interactions in HCV infection, a deeper understanding of which may aid in the identification of new clinically relevant targets for optimizing the therapeutic strategies to manipulate HCV−host interactions and thus more effectively combating HCV infection. Our analysis also emphasizes the importance of elaborate network-based computational approaches that integrate diverse biological data types in investigating host−pathogen interactions.

ASSOCIATED CONTENT

Supporting Information

Supporting methods, figures, and tables. This material is available free of charge via the Internet at http://pubs.acs.org.

AUTHOR INFORMATION

Corresponding Author

*E-mail: kenji@nibio.go.jp (K.M.); lokesh@nibio.go.jp (L.P.T.). Tel: +81-72-641-9890. Fax: +81-72-641-9881.

Author Contributions

¶L. P. Tripathi and H. Kambara contributed equally to this work.

Notes

The authors declare no competing financial interest.

ACKNOWLEDGMENTS

This study was supported by the Industrial Technology Research Grant Program in 2007 from New Energy and Industrial Technology Development Organization (NEDO) of Japan and also by grants-in-aid from the Ministry of Health, Labor, and Welfare; the Ministry of Education, Culture, Sports, Science, and Technology; the Osaka University Global Center of Excellence Program; and the Foundation for Biomedical Research and Innovation.

REFERENCES

(1) Dubuisson, J. Hepatitis C virus proteins. *World J. Gastroenterol.* **2007**, *13* (17), 2406−15.

(2) Moriishi, K.; Matsuura, Y. Host factors involved in the replication of hepatitis C virus. *Rev. Med. Virol.* **2007**, *17* (5), 343−54.

(3) Myrmel, H.; Ulvestad, E.; Asjo, B. The hepatitis C virus enigma. *APMIS* **2009**, *117* (5−6), 427−39.

(4) Tang, H.; Grise, H. Cellular and molecular biology of HCV infection and hepatitis. *Clin. Sci.* **2009**, *117* (2), 49−65.

(5) Pol, S.; Vallet-Pichard, A.; Corouge, M.; Mallet, V. O. Hepatitis C: epidemiology, diagnosis, natural history and therapy. *Contrib. Nephrol.* **2012**, *176*, 1−9.

(6) Kuiken, C.; Simmonds, P. Nomenclature and numbering of the hepatitis C virus. *Methods Mol. Biol.* **2009**, *510*, 33−53.

(7) Moradpour, D.; Penin, F.; Rice, C. M. Replication of hepatitis C virus. *Nat. Rev. Microbiol.* **2007**, *5* (6), 453−63.

(8) Love, R. A.; Brodsky, O.; Hickey, M. J.; Wells, P. A.; Cronin, C. N. Crystal structure of a novel dimeric form of NS5A domain I protein from hepatitis C virus. *J. Virol.* **2009**, *83* (9), 4395−403.

(9) Yamasaki, L. H.; Arcuri, H. A.; Jardim, A. C.; Bittar, C.; de Carvalho-Mello, I. M.; Rahal, P. New insights regarding HCV-NS5A structure/function and indication of genotypic differences. *Virol. J.* **2012**, *9*, 14.

(10) Appel, N.; Zayas, M.; Miller, S.; Krijnse-Locker, J.; Schaller, T.; Friebe, P.; Kallis, S.; Engel, U.; Bartenschlager, R. Essential role of domain III of nonstructural protein 5A for hepatitis C virus infectious particle assembly. *PLoS Pathog.* **2008**, *4* (3), e1000035.

(11) Gale, M. J., Jr.; Korth, M. J.; Tang, N. M.; Tan, S. L.; Hopkins, D. A.; Dever, T. E.; Polyak, S. J.; Gretch, D. R.; Katze, M. G. Evidence that hepatitis C virus resistance to interferon is mediated through repression of the PKR protein kinase by the nonstructural 5A protein. *Virology* **1997**, *230* (2), 217–27.
(12) Ghosh, S.; Ahrens, W. A.; Phatak, S. U.; Hwang, S.; Schrum, L. W.; Bonkovsky, H. L. Association of filamin A and vimentin with hepatitis C virus proteins in infected human hepatocytes. *J. Viral Hepatitis* **2011**, *18* (10), e568–77.
(13) Gao, M.; Nettles, R. E.; Belema, M.; Snyder, L. B.; Nguyen, V. N.; Fridell, R. A.; Serrano-Wu, M. H.; Langley, D. R.; Sun, J. H.; O'Boyle, D. R., 2nd; Lemm, J. A.; Wang, C.; Knipe, J. O.; Chien, C.; Colonno, R. J.; Grasela, D. M.; Meanwell, N. A.; Hamann, L. G. Chemical genetics strategy identifies an HCV NS5A inhibitor with a potent clinical effect. *Nature* **2010**, *465* (7294), 96–100.
(14) Lee, C. Discovery of hepatitis C virus NS5A inhibitors as a new class of anti-HCV therapy. *Arch. Pharmacal Res.* **2011**, *34* (9), 1403–7.
(15) Lemm, J. A.; O'Boyle, D., 2nd; Liu, M.; Nower, P. T.; Colonno, R.; Deshpande, M. S.; Snyder, L. B.; Martin, S. W.; St Laurent, D. R.; Serrano-Wu, M. H.; Romine, J. L.; Meanwell, N. A.; Gao, M. Identification of hepatitis C virus NS5A inhibitors. *J. Virol.* **2010**, *84* (1), 482–91.
(16) Lemon, S. M.; McKeating, J. A.; Pietschmann, T.; Frick, D. N.; Glenn, J. S.; Tellinghuisen, T. L.; Symons, J.; Furman, P. A. Development of novel therapies for hepatitis C. *Antiviral Res.* **2010**, *86* (1), 79–92.
(17) Fusco, D. N.; Chung, R. T. Novel therapies for hepatitis C: insights from the structure of the virus. *Annu. Rev. Med.* **2012**, *63*, 373–87.
(18) Buhler, S.; Bartenschlager, R. New targets for antiviral therapy of chronic hepatitis C. *Liver Int.* **2012**, *32* (Suppl 1), 9–16.
(19) Sarrazin, C.; Hezode, C.; Zeuzem, S.; Pawlotsky, J. M. Antiviral strategies in hepatitis C virus infection. *J. Hepatol.* **2012**, *56* (Suppl), S88–S100.
(20) Wang, S.; Wu, X.; Pan, T.; Song, W.; Wang, Y.; Zhang, F.; Yuan, Z. Viperin inhibits hepatitis C virus replication by interfering with binding of NS5A to host protein hVAP-33. *J. Gen. Virol.* **2012**, *93* (Pt1), 83–92.
(21) Durmus Tekir, S.; Cakir, T.; Ulgen, K. O. Infection strategies of bacterial and viral pathogens through pathogen-human protein-protein interactions. *Front. Microbiol.* **2012**, *3*, 46.
(22) de Chassey, B.; Navratil, V.; Tafforeau, L.; Hiet, M. S.; Aublin-Gex, A.; Agaugue, S.; Meiffren, G.; Pradezynski, F.; Faria, B. F.; Chantier, T.; Le Breton, M.; Pellet, J.; Davoust, N.; Mangeot, P. E.; Chaboud, A.; Penin, F.; Jacob, Y.; Vidalain, P. O.; Vidal, M.; Andre, P.; Rabourdin-Combe, C.; Lotteau, V. Hepatitis C virus infection protein network. *Mol. Syst. Biol.* **2008**, *4*, 230.
(23) Tan, S. L.; Ganji, G.; Paeper, B.; Proll, S.; Katze, M. G. Systems biology and the host response to viral infection. *Nat. Biotechnol.* **2007**, *25* (12), 1383–9.
(24) Tripathi, L. P.; Kataoka, C.; Taguwa, S.; Moriishi, K.; Mori, Y.; Matsuura, Y.; Mizuguchi, K. Network based analysis of hepatitis C virus Core and NS4B protein interactions. *Mol. BioSyst.* **2010**, *6* (12), 2539–53.
(25) Friedel, C. C.; Haas, J. Virus-host interactomes and global models of virus-infected cells. *Trends Microbiol.* **2011**, *19* (10), 501–8.
(26) Tafforeau, L.; Rabourdin-Combe, C.; Lotteau, V. Virus-human cell interactomes. *Methods Mol. Biol.* **2012**, *812*, 103–20.
(27) Aizaki, H.; Aoki, Y.; Harada, T.; Ishii, K.; Suzuki, T.; Nagamori, S.; Toda, G.; Matsuura, Y.; Miyamura, T. Full-length complementary DNA of hepatitis C virus genome from an infectious blood sample. *Hepatology* **1998**, *27* (2), 621–7.
(28) Hamamoto, I.; Nishimura, Y.; Okamoto, T.; Aizaki, H.; Liu, M.; Mori, Y.; Abe, T.; Suzuki, T.; Lai, M. M.; Miyamura, T.; Moriishi, K.; Matsuura, Y. Human VAP-B is involved in hepatitis C virus replication through interaction with NS5A and NS5B. *J. Virol.* **2005**, *79* (21), 13473–82.
(29) Rebholz-Schuhmann, D.; Kirsch, H.; Arregui, M.; Gaudan, S.; Riethoven, M.; Stoehr, P. EBIMed—text crunching to gather facts for proteins from Medline. *Bioinformatics* **2007**, *23* (2), e237–44.
(30) Rebholz-Schuhmann, D.; Arregui, M.; Gaudan, S.; Kirsch, H.; Jimeno, A. Text processing through Web services: calling Whatizit. *Bioinformatics* **2008**, *24* (2), 296–8.
(31) Stark, C.; Breitkreutz, B. J.; Reguly, T.; Boucher, L.; Breitkreutz, A.; Tyers, M. BioGRID: a general repository for interaction datasets. *Nucleic Acids Res.* **2006**, *34* (Database issue), D535–9.
(32) Turner, B.; Razick, S.; Turinsky, A. L.; Vlasblom, J.; Crowdy, E. K.; Cho, E.; Morrison, K.; Donaldson, I. M.; Wodak, S. J. iRefWeb: interactive analysis of consolidated protein interaction data and their supporting evidence. *Database* **2010**, *2010*, baq023.
(33) Chen, Y. A.; Tripathi, L. P.; Mizuguchi, K. TargetMine, an integrated data warehouse for candidate gene prioritisation and target discovery. *PLoS One* **2011**, *6* (3), e17844.
(34) Cline, M. S.; Smoot, M.; Cerami, E.; Kuchinsky, A.; Landys, N.; Workman, C.; Christmas, R.; Avila-Campilo, I.; Creech, M.; Gross, B.; Hanspers, K.; Isserlin, R.; Kelley, R.; Killcoyne, S.; Lotia, S.; Maere, S.; Morris, J.; Ono, K.; Pavlovic, V.; Pico, A. R.; Vailaya, A.; Wang, P. L.; Adler, A.; Conklin, B. R.; Hood, L.; Kuiper, M.; Sander, C.; Schmulevich, I.; Schwikowski, B.; Warner, G. J.; Ideker, T.; Bader, G. D. Integration of biological networks and gene expression data using Cytoscape. *Nat. Protoc.* **2007**, *2* (10), 2366–82.
(35) Smoot, M. E.; Ono, K.; Ruscheinski, J.; Wang, P. L.; Ideker, T. Cytoscape 2.8: new features for data integration and network visualization. *Bioinformatics* **2011**, *27* (3), 431–2.
(36) Assenov, Y.; Ramirez, F.; Schelhorn, S. E.; Lengauer, T.; Albrecht, M. Computing topological parameters of biological networks. *Bioinformatics* **2008**, *24* (2), 282–4.
(37) Lees, J.; Yeats, C.; Perkins, J.; Sillitoe, I.; Rentzsch, R.; Dessailly, B. H.; Orengo, C. Gene3D: a domain-based resource for comparative genomics, functional annotation and protein network analysis. *Nucleic Acids Res.* **2012**, *40* (Database issue), D465–71.
(38) Ashburner, M.; Ball, C. A.; Blake, J. A.; Botstein, D.; Butler, H.; Cherry, J. M.; Davis, A. P.; Dolinski, K.; Dwight, S. S.; Eppig, J. T.; Harris, M. A.; Hill, D. P.; Issel-Tarver, L.; Kasarskis, A.; Lewis, S.; Matese, J. C.; Richardson, J. E.; Ringwald, M.; Rubin, G. M.; Sherlock, G. Gene ontology: tool for the unification of biology. The Gene Ontology Consortium. *Nat. Genet.* **2000**, *25* (1), 25–9.
(39) Aoki-Kinoshita, K. F.; Kanehisa, M. Gene annotation and pathway mapping in KEGG. *Methods Mol. Biol.* **2007**, *396*, 71–91.
(40) Benjamini, Y.; Hochberg, Y. Controlling the false discovery rate—A practical and powerful approach to multiple testing. *J. R. Stat. Soc. B* **1995**, *57* (1), 289–300.
(41) Noble, W. S. How does multiple testing correction work? *Nat. Biotechnol.* **2009**, *27* (12), 1135–7.
(42) Okamoto, K.; Mori, Y.; Komoda, Y.; Okamoto, T.; Okochi, M.; Takeda, M.; Suzuki, T.; Moriishi, K.; Matsuura, Y. Intramembrane processing by signal peptide peptidase regulates the membrane localization of hepatitis C virus core protein and viral propagation. *J. Virol.* **2008**, *82* (17), 8349–61.
(43) Okamoto, T.; Omori, H.; Kaname, Y.; Abe, T.; Nishimura, Y.; Suzuki, T.; Miyamura, T.; Yoshimori, T.; Moriishi, K.; Matsuura, Y. A single-amino-acid mutation in hepatitis C virus NS5A disrupting FKBP8 interaction impairs viral replication. *J. Virol.* **2008**, *82* (7), 3480–9.
(44) Wakita, T.; Pietschmann, T.; Kato, T.; Date, T.; Miyamoto, M.; Zhao, Z.; Murthy, K.; Habermann, A.; Krausslich, H. G.; Mizokami, M.; Bartenschlager, R.; Liang, T. J. Production of infectious hepatitis C virus in tissue culture from a cloned viral genome. *Nat. Med.* **2005**, *11* (7), 791–6.
(45) Taguwa, S.; Kambara, H.; Omori, H.; Tani, H.; Abe, T.; Mori, Y.; Suzuki, T.; Yoshimori, T.; Moriishi, K.; Matsuura, Y. Cochaperone activity of human butyrate-induced transcript 1 facilitates hepatitis C virus replication through an Hsp90-dependent pathway. *J. Virol.* **2009**, *83* (20), 10427–36.
(46) Kukihara, H.; Moriishi, K.; Taguwa, S.; Tani, H.; Abe, T.; Mori, Y.; Suzuki, T.; Fukuhara, T.; Taketomi, A.; Maehara, Y.; Matsuura, Y.

Human VAP-C negatively regulates hepatitis C virus propagation. *J. Virol.* **2009**, *83* (16), 7959–69.
(47) Nanda, S. K.; Herion, D.; Liang, T. J. The SH3 binding motif of HCV [corrected] NS5A protein interacts with Bin1 and is important for apoptosis and infectivity. *Gastroenterology* **2006**, *130* (3), 794–809.
(48) Liu, A. W.; Cai, J.; Zhao, X. L.; Jiang, T. H.; He, T. F.; Fu, H. Q.; Zhu, M. H.; Zhang, S. H. ShRNA-targeted MAP4K4 inhibits hepatocellular carcinoma growth. *Clin. Cancer Res.* **2011**, *17* (4), 710–20.
(49) Woodhouse, S. D.; Narayan, R.; Latham, S.; Lee, S.; Antrobus, R.; Gangadharan, B.; Luo, S.; Schroth, G. P.; Klenerman, P.; Zitzmann, N. Transcriptome sequencing, microarray, and proteomic analyses reveal cellular and metabolic impact of hepatitis C virus infection in vitro. *Hepatology* **2010**, *52* (2), 443–53.
(50) MacPherson, J. I.; Sidders, B.; Wieland, S.; Zhong, J.; Targett-Adams, P.; Lohmann, V.; Backes, P.; Delpuech-Adams, O.; Chisari, F.; Lewis, M.; Parkinson, T.; Robertson, D. L. An integrated transcriptomic and meta-analysis of hepatoma cells reveals factors that influence susceptibility to HCV infection. *PLoS One* **2011**, *6* (10), e25584.
(51) Yamashita, T.; Honda, M.; Kaneko, S. Molecular mechanisms of hepatocarcinogenesis in chronic hepatitis C virus infection. *J. Gastroenterol. Hepatol.* **2011**, *26* (6), 960–4.
(52) Yu, H.; Kim, P. M.; Sprecher, E.; Trifonov, V.; Gerstein, M. The importance of bottlenecks in protein networks: correlation with gene essentiality and expression dynamics. *PLoS Comput. Biol.* **2007**, *3* (4), e59.
(53) Rasmussen, A. L.; Diamond, D. L.; McDermott, J. E.; Gao, X.; Metz, T. O.; Matzke, M. M.; Carter, V. S.; Belisle, S. E.; Korth, M. J.; Waters, K. M.; Smith, R. D.; Katze, M. G. Systems virology identifies a mitochondrial fatty acid oxidation enzyme, dodecenoyl coenzyme A delta isomerase, required for hepatitis C virus replication and likely pathogenesis. *J. Virol.* **2011**, *85* (22), 11646–54.
(54) Diamond, D. L.; Krasnoselsky, A. L.; Burnum, K. E.; Monroe, M. E.; Webb-Robertson, B. J.; McDermott, J. E.; Yeh, M. M.; Dzib, J. F.; Susnow, N.; Strom, S.; Proll, S. C.; Belisle, S. E.; Purdy, D. E.; Rasmussen, A. L.; Walters, K. A.; Jacobs, J. M.; Gritsenko, M. A.; Camp, D. G.; Bhattacharya, R.; Perkins, J. D.; Carithers, R. L., Jr.; Liou, I. W.; Larson, A. M.; Benecke, A.; Waters, K. M.; Smith, R. D.; Katze, M. G. Proteome and computational analyses reveal new insights into the mechanisms of hepatitis C virus-mediated liver disease posttransplantation. *Hepatology* **2012**, *56* (1), 28–38.
(55) He, Y.; Nakao, H.; Tan, S. L.; Polyak, S. J.; Neddermann, P.; Vijaysri, S.; Jacobs, B. L.; Katze, M. G. Subversion of cell signaling pathways by hepatitis C virus nonstructural 5A protein via interaction with Grb2 and P85 phosphatidylinositol 3-kinase. *J. Virol.* **2002**, *76* (18), 9207–17.
(56) Jiang, Y. F.; He, B.; Li, N. P.; Ma, J.; Gong, G. Z.; Zhang, M. The oncogenic role of NS5A of hepatitis C virus is mediated by up-regulation of survivin gene expression in the hepatocellular cell through p53 and NF-kappaB pathways. *Cell Biol. Int.* **2011**, *35* (12), 1225–32.
(57) Pfannkuche, A.; Buther, K.; Karthe, J.; Poenisch, M.; Bartenschlager, R.; Trilling, M.; Hengel, H.; Willbold, D.; Haussinger, D.; Bode, J. G. c-Src is required for complex formation between the hepatitis C virus-encoded proteins NS5A and NS5B: a prerequisite for replication. *Hepatology* **2011**, *53* (4), 1127–36.
(58) Calderwood, M. A.; Venkatesan, K.; Xing, L.; Chase, M. R.; Vazquez, A.; Holthaus, A. M.; Ewence, A. E.; Li, N.; Hirozane-Kishikawa, T.; Hill, D. E.; Vidal, M.; Kieff, E.; Johannsen, E. Epstein-Barr virus and virus human protein interaction maps. *Proc. Natl. Acad. Sci. U. S. A.* **2007**, *104* (18), 7606–11.
(59) Pichlmair, A.; Kandasamy, K.; Alvisi, G.; Mulhern, O.; Sacco, R.; Habjan, M.; Binder, M.; Stefanovic, A.; Eberle, C. A.; Goncalves, A.; Burckstummer, T.; Muller, A. C.; Fauster, A.; Holze, C.; Lindsten, K.; Goodbourn, S.; Kochs, G.; Weber, F.; Bartenschlager, R.; Bowie, A. G.; Bennett, K. L.; Colinge, J.; Superti-Furga, G. Viral immune modulators perturb the human molecular network by common and unique strategies. *Nature* **2012**, *487* (7408), 486–90.
(60) Huang, H.; Jedynak, B. M.; Bader, J. S. Where have all the interactions gone? Estimating the coverage of two-hybrid protein interaction maps. *PLoS Comput. Biol.* **2007**, *3* (11), e214.
(61) Nordle Gilliver, A.; Griffin, S.; Harris, M. Identification of a novel phosphorylation site in hepatitis C virus NS5A. *J. Gen. Virol.* **2010**, *91* (Pt 10), 2428–32.
(62) Qiu, D.; Lemm, J. A.; O'Boyle, D. R., 2nd; Sun, J. H.; Nower, P. T.; Nguyen, V.; Hamann, L. G.; Snyder, L. B.; Deon, D. H.; Ruediger, E.; Meanwell, N. A.; Belema, M.; Gao, M.; Fridell, R. A. The effects of NS5A inhibitors on NS5A phosphorylation, polyprotein processing and localization. *J. Gen. Virol.* **2011**, *92* (Pt11), 2502–11.
(63) Tellinghuisen, T. L.; Foss, K. L.; Treadaway, J. Regulation of hepatitis C virion production via phosphorylation of the NS5A protein. *PLoS Pathog.* **2008**, *4* (3), e1000032.
(64) Chen, K. C.; Wang, T. Y.; Chan, C. H. Associations between HIV and human pathways revealed by protein-protein interactions and correlated gene expression profiles. *PLoS One* **2012**, *7* (3), e34240.
(65) Rozenblatt-Rosen, O.; Deo, R. C.; Padi, M.; Adelmant, G.; Calderwood, M. A.; Rolland, T.; Grace, M.; Dricot, A.; Askenazi, M.; Tavares, M.; Pevzner, S. J.; Abderazzaq, F.; Byrdsong, D.; Carvunis, A. R.; Chen, A. A.; Cheng, J.; Correll, M.; Duarte, M.; Fan, C.; Feltkamp, M. C.; Ficarro, S. B.; Franchi, R.; Garg, B. K.; Gulbahce, N.; Hao, T.; Holthaus, A. M.; James, R.; Korkhin, A.; Litovchick, L.; Mar, J. C.; Pak, T. R.; Rabello, S.; Rubio, R.; Shen, Y.; Singh, S.; Spangle, J. M.; Tasan, M.; Wanamaker, S.; Webber, J. T.; Roecklein-Canfield, J.; Johannsen, E.; Barabasi, A. L.; Beroukhim, R.; Kieff, E.; Cusick, M. E.; Hill, D. E.; Munger, K.; Marto, J. A.; Quackenbush, J.; Roth, F. P.; DeCaprio, J. A.; Vidal, M. Interpreting cancer genomes using systematic host network perturbations by tumour virus proteins. *Nature* **2012**, *487* (7408), 491–5.
(66) Barnaba, V. Hepatitis C virus infection: a "liaison a trois" amongst the virus, the host, and chronic low-level inflammation for human survival. *J. Hepatol.* **2010**, *53* (4), 752–61.
(67) Hiroishi, K.; Ito, T.; Imawari, M. Immune responses in hepatitis C virus infection and mechanisms of hepatitis C virus persistence. *J. Gastroenterol. Hepatol.* **2008**, *23* (10), 1473–82.
(68) Kawai, T.; Akira, S. Toll-like receptor and RIG-I-like receptor signaling. *Ann. N. Y. Acad. Sci.* **2008**, *1143*, 1–20.
(69) Sklan, E. H.; Charuworn, P.; Pang, P. S.; Glenn, J. S. Mechanisms of HCV survival in the host. *Nat. Rev. Gastroenterol. Hepatol.* **2009**, *6* (4), 217–27.
(70) Kang, S. M.; Won, S. J.; Lee, G. H.; Lim, Y. S.; Hwang, S. B. Modulation of interferon signaling by hepatitis C virus non-structural 5A protein: implication of genotypic difference in interferon treatment. *FEBS Lett.* **2010**, *584* (18), 4069–76.
(71) Li, K.; Li, N. L.; Wei, D.; Pfeffer, S. R.; Fan, M.; Pfeffer, L. M. Activation of chemokine and inflammatory cytokine response in hepatitis C virus-infected hepatocytes depends on Toll-like receptor 3 sensing of hepatitis C virus double-stranded RNA intermediates. *Hepatology* **2012**, *55* (3), 666–75.
(72) Tanaka, S.; Arii, S. Molecularly targeted therapy for hepatocellular carcinoma. *Cancer Sci.* **2009**, *100* (1), 1–8.
(73) Tanaka, S.; Arii, S. Current status of molecularly targeted therapy for hepatocellular carcinoma: basic science. *Int. J. Clin. Oncol.* **2010**, *15* (3), 235–41.
(74) Villanueva, A.; Chiang, D. Y.; Newell, P.; Peix, J.; Thung, S.; Alsinet, C.; Tovar, V.; Roayaie, S.; Minguez, B.; Sole, M.; Battiston, C.; Van Laarhoven, S.; Fiel, M. I.; Di Feo, A.; Hoshida, Y.; Yea, S.; Toffanin, S.; Ramos, A.; Martignetti, J. A.; Mazzaferro, V.; Bruix, J.; Waxman, S.; Schwartz, M.; Meyerson, M.; Friedman, S. L.; Llovet, J. M. Pivotal role of mTOR signaling in hepatocellular carcinoma. *Gastroenterology* **2008**, *135* (6), 1972–83.
(75) Cheng, D.; Zhao, L.; Zhang, L.; Jiang, Y.; Tian, Y.; Xiao, X.; Gong, G. p53 controls hepatitis C virus non-structural protein 5A-mediated downregulation of GADD45alpha expression via the NF-kappaB and PI3K-Akt pathways. *J. Gen. Virol.* **2013**, *94* (Pt 2), 326–35.
(76) Tripathi, L. P.; Kambara, H.; Moriishi, K.; Morita, E.; Abe, T.; Mori, Y.; Chen, Y. A.; Matsuura, Y.; Mizuguchi, K. Proteomic analysis

of hepatitis C virus (HCV) core protein transfection and host regulator PA28gamma knockout in HCV pathogenesis: a network-based study. *J. Proteome Res.* **2012**, *11* (7), 3664–79.
(77) Zhao, L. J.; Zhao, P.; Chen, Q. L.; Ren, H.; Pan, W.; Qi, Z. T. Mitogen-activated protein kinase signalling pathways triggered by the hepatitis C virus envelope protein E2: implications for the prevention of infection. *Cell Proliferation* **2007**, *40* (4), 508–21.
(78) Basaranoglu, M.; Basaranoglu, G. Pathophysiology of insulin resistance and steatosis in patients with chronic viral hepatitis. *World J. Gastroenterol.* **2011**, *17* (36), 4055–62.
(79) Del Campo, J. A.; Romero-Gomez, M. Steatosis and insulin resistance in hepatitis C: a way out for the virus? *World J. Gastroenterol.* **2009**, *15* (40), 5014–9.
(80) Douglas, M. W.; George, J. Molecular mechanisms of insulin resistance in chronic hepatitis C. *World J. Gastroenterol.* **2009**, *15* (35), 4356–64.
(81) Das, G. C.; Hollinger, F. B. Molecular pathways for glucose homeostasis, insulin signaling and autophagy in hepatitis C virus induced insulin resistance in a cellular model. *Virology* **2012**, *434* (1), 5–17.
(82) Miyamoto, H.; Moriishi, K.; Moriya, K.; Murata, S.; Tanaka, K.; Suzuki, T.; Miyamura, T.; Koike, K.; Matsuura, Y. Involvement of the PA28gamma-dependent pathway in insulin resistance induced by hepatitis C virus core protein. *J. Virol.* **2007**, *81* (4), 1727–35.
(83) Kaneko, K.; Ueki, K.; Takahashi, N.; Hashimoto, S.; Okamoto, M.; Awazawa, M.; Okazaki, Y.; Ohsugi, M.; Inabe, K.; Umehara, T.; Yoshida, M.; Kakei, M.; Kitamura, T.; Luo, J.; Kulkarni, R. N.; Kahn, C. R.; Kasai, H.; Cantley, L. C.; Kadowaki, T. Class IA phosphatidylinositol 3-kinase in pancreatic beta cells controls insulin secretion by multiple mechanisms. *Cell Metab.* **2010**, *12* (6), 619–32.
(84) Milward, A.; Mankouri, J.; Harris, M. Hepatitis C virus NS5A protein interacts with beta-catenin and stimulates its transcriptional activity in a phosphoinositide-3 kinase-dependent fashion. *J. Gen. Virol.* **2010**, *91* (Pt 2), 373–81.
(85) Alberstein, M.; Zornitzki, T.; Zick, Y.; Knobler, H. Hepatitis C core protein impairs insulin downstream signalling and regulatory role of IGFBP-1 expression. *J. Viral Hepatitis* **2012**, *19* (1), 65–71.
(86) Benedicto, I.; Molina-Jimenez, F.; Bartosch, B.; Cosset, F. L.; Lavillette, D.; Prieto, J.; Moreno-Otero, R.; Valenzuela-Fernandez, A.; Aldabe, R.; Lopez-Cabrera, M.; Majano, P. L. The tight junction-associated protein occludin is required for a postbinding step in hepatitis C virus entry and infection. *J. Virol.* **2009**, *83* (16), 8012–20.
(87) Carloni, G.; Crema, A.; Valli, M. B.; Ponzetto, A.; Clementi, M. HCV infection by cell-to-cell transmission: choice or necessity? *Curr. Mol. Med.* **2012**, *12* (1), 83–95.
(88) Wilson, G. K.; Brimacombe, C. L.; Rowe, I. A.; Reynolds, G. M.; Fletcher, N. F.; Stamataki, Z.; Bhogal, R. H.; Simoes, M. L.; Ashcroft, M.; Afford, S. C.; Mitry, R. R.; Dhawan, A.; Mee, C. J.; Hubscher, S. G.; Balfe, P.; McKeating, J. A. A dual role for hypoxia inducible factor-1alpha in the hepatitis C virus lifecycle and hepatoma migration. *J. Hepatol.* **2012**, *56* (4), 803–9.
(89) Daugherty, R. L.; Gottardi, C. J. Phospho-regulation of beta-catenin adhesion and signaling functions. *Physiology* **2007**, *22*, 303–9.
(90) Presser, L. D.; Haskett, A.; Waris, G. Hepatitis C virus-induced furin and thrombospondin-1 activate TGF-beta1: role of TGF-beta1 in HCV replication. *Virology* **2011**, *412* (2), 284–96.
(91) Berger, K. L.; Cooper, J. D.; Heaton, N. S.; Yoon, R.; Oakland, T. E.; Jordan, T. X.; Mateu, G.; Grakoui, A.; Randall, G. Roles for endocytic trafficking and phosphatidylinositol 4-kinase III alpha in hepatitis C virus replication. *Proc. Natl. Acad. Sci. U. S. A.* **2009**, *106* (18), 7577–82.
(92) Katsarou, K.; Lavdas, A. A.; Tsitoura, P.; Serti, E.; Markoulatos, P.; Mavromara, P.; Georgopoulou, U. Endocytosis of hepatitis C virus non-enveloped capsid-like particles induces MAPK-ERK1/2 signaling events. *Cell. Mol. Life Sci.* **2010**, *67*, 2491–506.
(93) Mankouri, J.; Griffin, S.; Harris, M. The hepatitis C virus non-structural protein NS5A alters the trafficking profile of the epidermal growth factor receptor. *Traffic* **2008**, *9* (9), 1497–509.
(94) Diao, J.; Pantua, H.; Ngu, H.; Komuves, L.; Diehl, L.; Schaefer, G.; Kapadia, S. B. Hepatitis C virus (HCV) induces epidermal growth factor receptor (EGFR) activation via CD81 binding for viral internalization and entry. *J. Virol.* **2012**, *86* (20), 10935–49.
(95) Yoon, H. Y.; Kales, S. C.; Luo, R.; Lipkowitz, S.; Randazzo, P. A. ARAP1 association with CIN85 affects epidermal growth factor receptor endocytic trafficking. *Biol. Cell* **2011**, *103* (4), 171–84.
(96) Katsarou, K.; Lavdas, A. A.; Tsitoura, P.; Serti, E.; Markoulatos, P.; Mavromara, P.; Georgopoulou, U. Endocytosis of hepatitis C virus non-enveloped capsid-like particles induces MAPK-ERK1/2 signaling events. *Cell. Mol. Life Sci.* **2010**, *67* (14), 2491–506.
(97) Diaz, A.; Ahlquist, P. Role of host reticulon proteins in rearranging membranes for positive-strand RNA virus replication. *Curr. Opin. Microbiol.* **2012**, *15* (4), 519–24.
(98) Diaz, A.; Wang, X.; Ahlquist, P. Membrane-shaping host reticulon proteins play crucial roles in viral RNA replication compartment formation and function. *Proc. Natl. Acad. Sci. U. S. A.* **2010**, *107* (37), 16291–6.
(99) Rahim, A.; Nafi-valencia, E.; Siddiqi, S.; Basha, R.; Runyon, C. C.; Siddiqi, S. A. Proteomic analysis of the very low density lipoprotein (VLDL) transport vesicles. *J Proteomics* **2012**, *75* (7), 2225–35.
(100) Coller, K. E.; Heaton, N. S.; Berger, K. L.; Cooper, J. D.; Saunders, J. L.; Randall, G. Molecular determinants and dynamics of hepatitis C virus secretion. *PLoS Pathog.* **2012**, *8* (1), e1002466.
(101) Lai, C. K.; Jeng, K. S.; Machida, K.; Lai, M. M. Association of hepatitis C virus replication complexes with microtubules and actin filaments is dependent on the interaction of NS3 and NS5A. *J. Virol.* **2008**, *82* (17), 8838–48.
(102) Randall, G.; Panis, M.; Cooper, J. D.; Tellinghuisen, T. L.; Sukhodolets, K. E.; Pfeffer, S.; Landthaler, M.; Landgraf, P.; Kan, S.; Lindenbach, B. D.; Chien, M.; Weir, D. B.; Russo, J. J.; Ju, J.; Brownstein, M. J.; Sheridan, R.; Sander, C.; Zavolan, M.; Tuschl, T.; Rice, C. M. Cellular cofactors affecting hepatitis C virus infection and replication. *Proc. Natl. Acad. Sci. U. S. A.* **2007**, *104* (31), 12884–9.
(103) Saxena, V.; Lai, C. K.; Chao, T. C.; Jeng, K. S.; Lai, M. M. Annexin A2 is involved in the formation of hepatitis C virus replication complex on the lipid raft. *J. Virol.* **2012**, *86* (8), 4139–50.
(104) Quintavalle, M.; Sambucini, S.; Summa, V.; Orsatti, L.; Talamo, F.; De Francesco, R.; Neddermann, P. Hepatitis C virus NS5A is a direct substrate of casein kinase I-alpha, a cellular kinase identified by inhibitor affinity chromatography using specific NS5A hyperphosphorylation inhibitors. *J. Biol. Chem.* **2007**, *282* (8), 5536–44.
(105) Ivanov, A. V.; Tunitskaya, V. L.; Ivanova, O. N.; Mitkevich, V. A.; Prassolov, V. S.; Makarov, A. A.; Kukhanova, M. K.; Kochetkov, S. N. Hepatitis C virus NS5A protein modulates template selection by the RNA polymerase in in vitro system. *FEBS Lett.* **2009**, *583* (2), 277–80.
(106) Park, C. Y.; Choi, S. H.; Kang, S. M.; Kang, J. I.; Ahn, B. Y.; Kim, H.; Jung, G.; Choi, K. Y.; Hwang, S. B. Nonstructural 5A protein activates beta-catenin signaling cascades: implication of hepatitis C virus-induced liver pathogenesis. *J. Hepatol.* **2009**, *51* (5), 853–64.
(107) Zhang, Z.; Harris, D.; Pandey, V. N. The FUSE binding protein is a cellular factor required for efficient replication of hepatitis C virus. *J. Virol.* **2008**, *82* (12), 5761–73.
(108) Chen, Y. J.; Chen, Y. H.; Chow, L. P.; Tsai, Y. H.; Chen, P. H.; Huang, C. Y.; Chen, W. T.; Hwang, L. H. Heat shock protein 72 is associated with the hepatitis C virus replicase complex and enhances viral RNA replication. *J. Biol. Chem.* **2010**, *285* (36), 28183–90.
(109) Choi, Y. W.; Tan, Y. J.; Lim, S. G.; Hong, W.; Goh, P. Y. Proteomic approach identifies HSP27 as an interacting partner of the hepatitis C virus NS5A protein. *Biochem. Biophys. Res. Commun.* **2004**, *318* (2), 514–9.
(110) Ahn, J.; Chung, K. S.; Kim, D. U.; Won, M.; Kim, L.; Kim, K. S.; Nam, M.; Choi, S. J.; Kim, H. C.; Yoon, M.; Chae, S. K.; Hoe, K. L. Systematic identification of hepatocellular proteins interacting with NS5A of the hepatitis C virus. *J. Biochem. Mol. Biol.* **2004**, *37* (6), 741–8.

(111) Amako, Y.; Sarkeshik, A.; Hotta, H.; Yates, J., 3rd; Siddiqui, A. Role of oxysterol binding protein in hepatitis C virus infection. *J. Virol.* **2009**, *83* (18), 9237–46.
(112) Lim, Y. S.; Tran, H. T.; Park, S. J.; Yim, S. A.; Hwang, S. B. Peptidyl-prolyl isomerase Pin1 is a cellular factor required for hepatitis C virus propagation. *J. Virol.* **2011**, *85* (17), 8777–88.
(113) Chen, Y. C.; Su, W. C.; Huang, J. Y.; Chao, T. C.; Jeng, K. S.; Machida, K.; Lai, M. M. Polo-like kinase 1 is involved in hepatitis C virus replication by hyperphosphorylating NS5A. *J. Virol.* **2010**, *84* (16), 7983–93.
(114) Waller, H.; Chatterji, U.; Gallay, P.; Parkinson, T.; Targett-Adams, P. The use of AlphaLISA technology to detect interaction between hepatitis C virus-encoded NS5A and cyclophilin A. *J. Virol. Methods* **2010**, *165* (2), 202–10.
(115) Chatterji, U.; Lim, P.; Bobardt, M. D.; Wieland, S.; Cordek, D. G.; Vuagniaux, G.; Chisari, F.; Cameron, C. E.; Targett-Adams, P.; Parkinson, T.; Gallay, P. A. HCV resistance to cyclosporin A does not correlate with a resistance of the NS5A-cyclophilin A interaction to cyclophilin inhibitors. *J. Hepatol.* **2010**, *53* (1), 50–6.
(116) Georgopoulou, U.; Tsitoura, P.; Kalamvoki, M.; Mavromara, P. The protein phosphatase 2A represents a novel cellular target for hepatitis C virus NS5A protein. *Biochimie* **2006**, *88* (6), 651–62.
(117) Helbig, K. J.; Eyre, N. S.; Yip, E.; Narayana, S.; Li, K.; Fiches, G.; McCartney, E. M.; Jangra, R. K.; Lemon, S. M.; Beard, M. R. The antiviral protein viperin inhibits hepatitis C virus replication via interaction with nonstructural protein 5A. *Hepatology* **2011**, *54* (5), 1506–17.
(118) Kumthip, K.; Chusri, P.; Jilg, N.; Zhao, L.; Fusco, D. N.; Zhao, H.; Goto, K.; Cheng, D.; Schaefer, E. A.; Zhang, L.; Pantip, C.; Thongsawat, S.; O'Brien, A.; Peng, L. F.; Maneekarn, N.; Chung, R. T.; Lin, W. Hepatitis C virus NS5A disrupts STAT1 phosphorylation and suppresses type I interferon signaling. *J. Virol.* **2012**, *86* (16), 8581–91.
(119) Inubushi, S.; Nagano-Fujii, M.; Kitayama, K.; Tanaka, M.; An, C.; Yokozaki, H.; Yamamura, H.; Nuriya, H.; Kohara, M.; Sada, K.; Hotta, H. Hepatitis C virus NS5A protein interacts with and negatively regulates the non-receptor protein tyrosine kinase Syk. *J. Gen. Virol.* **2008**, *89* (Pt 5), 1231–42.

ANTIOXIDANTS & REDOX SIGNALING
Volume 00, Number 00, 2013

DOI: 10.1089/ars.2013.5381

ORIGINAL RESEARCH COMMUNICATION

Nitrosative Stress Induces Peroxiredoxin 1 Ubiquitination During Ischemic Insult *via* E6AP Activation in Endothelial Cells Both *In Vitro* and *In Vivo*

Rong-Rong Tao,[1,*] Huan Wang,[1,*] Ling-Juan Hong,[1] Ji-Yun Huang,[1] Ying-Mei Lu,[2] Mei-Hua Liao,[1] Wei-Feng Ye,[1,3] Nan-Nan Lu,[1] Dan-Yan Zhu,[1] Qian Huang,[4] Kohji Fukunaga,[5] Yi-Jia Lou,[1] Ikuo Shoji,[6] Christopher Stuart Wilcox,[7] En-Yin Lai,[4,7] and Feng Han[1]

Abstract

Aims: Although there is accumulating evidence that increased formation of reactive nitrogen species in cerebral vasculature contributes to the progression of ischemic damage, but the underlying molecular mechanisms remain elusive. Peroxiredoxin 1 (Prx1) can initiate the antioxidant response by scavenging free radicals. Therefore, we tested the hypothesis that Prx1 regulates the susceptibility to nitrosative stress damage during cerebral ischemia *in vitro* and *in vivo*. ***Results:*** Proteomic analysis in endothelial cells revealed that Prx1 was upregulated after stress-related oxygen–glucose deprivation (OGD). Although peroxynitrite upregulated Prx1 rapidly, this was followed by its polyubiquitination within 6 h after OGD mediated by the E3 ubiquitin ligase E6-associated protein (E6AP). OGD colocalized E6AP with nitrotyrosine in endothelial cells. To assess translational relevance *in vivo*, mice were studied after middle cerebral artery occlusion (MCAO). This was accompanied by Prx1 ubiquitination and degradation by the activation of E6AP. Furthermore, brain delivery of a lentiviral vector encoding *Prx1* in mice inhibited blood–brain barrier leakage and neuronal damage significantly following MCAO. ***Innovation and Conclusions:*** Nitrosative stress during ischemic insult activates E6AP E3 ubiquitin ligase that ubiquitinates Prx1 and subsequently worsens cerebral damage. Thus, targeting the Prx1 antioxidant defense pathway may represent a novel treatment strategy for neurovascular protection in stroke. *Antioxid. Redox Signal.* 00, 000–000.

Introduction

BRAIN MICROVASCULAR ENDOTHELIAL CELLS provide a barrier between the bloodstream and brain that is critical in brain development, maturation, and homeostasis (9, 37). The balance between endothelial cell survival and death is pivotal for brain remodeling and repair (41). Increased cell death of cerebrovascular endothelial cells exacerbates inflammatory, ischemic, and degenerative brain diseases (26). Before a new strategy can be developed to counter these adverse effects of ischemia-induced endothelial dysfunction and neurovascular damage, it is necessary to define the factors responsible for ischemia-induced blood–brain barrier (BBB) damage.

Under conditions of intense oxidative stress, such as ischemia or hypoxia injury, increased generation of nitric oxide (NO) and superoxide ($O_2^{\bullet -}$) results in the formation of peroxynitrite ($ONOO^-$) (50). This is a short-lived highly reactive oxidant that attacks and inactivates many proteins. Specifically, $ONOO^-$ irreversibly inactivates prostacyclin

[1]Institute of Pharmacology, Toxicology and Biochemical Pharmaceutics, Zhejiang University, Hangzhou, China.
[2]School of Medicine, Zhejiang University City College, Hangzhou, Zhejiang, China.
[3]The Children's Hospital, Zhejiang University School of Medicine, Hangzhou, China.
[4]Department of Physiology, Zhejiang University School of Medicine, Hangzhou, China.
[5]Department of Pharmacology, Graduate School of Pharmaceutical Sciences, Tohoku University, Sendai, Japan.
[6]Division of Microbiology, Center for Infectious Diseases, Kobe University Graduate School of Medicine, Kobe, Japan.
[7]Hypertension, Kidney, and Vascular Research Center, Georgetown University Medical Center, Washington, District of Columbia.
*Both authors contributed equally to this work.

Innovation

Our study is the first demonstration that nitrosative stress initiates the ubiquitination of peroxiredoxin 1 (Prx1) and subsequent disturbance of redox homeostasis in endothelial cells during ischemia-like injury. Our findings further identified E6-associated protein (E6AP) E3 ligase that ubiquitinated Prx1. Thus, repression of peroxynitrite ($ONOO^-$) formation or *E6AP* knockdown dampened the ischemia-induced disturbance of Prx1 defense signaling. Since an active Prx1 was required for optimal neurovascular cell survival, targeting the Prx1 antioxidant defense pathway may represent a novel treatment strategy for neurovascular protection after stroke.

synthase and oxidizes tetrahydrabiopterin to dihydrabiopterin, thereby uncoupling endothelial NO synthase and directing it to generate $O_2^{\bullet -}$ in place of NO. Indeed, endothelial cells are the primary targets of nitrosative stress in cardiovascular disease, stroke, and neurodegenerative disorders (18, 48). Although nitrosative damage to lipids, proteins, and DNA has been implicated in neurovascular damage following cerebral ischemia, the downstream signaling mechanisms remain elusive (13, 16, 17, 29).

Peroxiredoxins (Prxs) are thiol-specific antioxidant enzymes that maintain redox balance under both normal conditions and oxidative stress (6, 7, 10, 28). Although Prx1 is the most abundant and widely distributed member of the mammalian Prxs (23, 24) and is a recognized peroxide-detoxifying enzyme, its pathophysiological role during brain disease remains unclear (38, 44). Cultured *Prx1*-deficient fibroblasts have decreased proliferation and increased sensitivity to oxidative DNA damage. *Prx1*-deficient mice developed hemolytic anemia caused by increased erythrocytic reactive oxygen species (ROS) (34). Furthermore, mutant Hungtington (*mHtt*) gene expression decreased Prx1 levels and increased its sulfonylation (35).

We tested the hypothesis that Prx1 in endothelial cells in culture and in the brain *in vivo* is a pivotal antioxidant pathway but can be damaged by nitrosative stress during hypoxia or ischemia, thereby exacerbating injury. We report that oxygen/glucose-deprived endothelial cells ubiquitinate Prx1 by nitrosative activation of E3 ubiquitin ligase (E6-associated protein [E6AP]). The outcome is that Prx1 is targeted for degradation leading to cellular redox imbalance and loss of the integrity of the endothelial BBB in mice following ischemia. Repression of $ONOO^-$ formation or *E6AP* knockdown dampened these disturbances of Prx1 defense signaling in endothelial cells. The initial study was made in human umbilical vascular endothelial cells, and key observations were confirmed and extended in human brain microvascular endothelial cells (HBMECs). Thus, our results indicate that Prx1 is a pivotal molecule for the protection of endothelial cells and microvessels from ischemia-induced neurovascular damage both *in vitro* and *in vivo*.

Results

Identification of differentially expressed proteins after oxygen–glucose deprivation in endothelial cells

Two-dimensional gel electrophoresis was performed in EA.hy926 endothelial cells to identify proteins that were differentially expressed between control and oxygen–glucose deprivation (OGD)-treated endothelial cells. Figure 1A shows a silver-stained two-dimensional gel electrophoresis reference map of the OGD-treated endothelial cultures (Fig. 1A, $n=3$, lower) in comparison to the control profile (Fig. 1A, $n=3$, upper). The spots that showed a twofold or greater difference between treatments were further characterized by trypsin digestion and matrix-assisted laser desorption/ionization (MALDI) time-of-flight (TOF) mass spectrometry. Twenty-two different proteins from 36 spots were identified with high confidence (CI % ranging from 97.5% to 100%) (Supplementary Table S1; Supplementary Data are available online at www.liebertpub.com/ars). The identified proteins were classified into functional groups (Supplementary Fig. S1). We selected Prx1 for further study since it was implicated in oxidation–reduction balance and abundantly increased 2.5-fold after OGD treatment (Supplementary Fig. S2A).

Temporal changes of Prx1 protein levels in endothelial cells after OGD

Immunoblotting studies demonstrated a time-dependent increase in Prx1 over 1–6 h followed by a decline after 12 h (Fig. 1B, C). There was a similar pattern of protein levels of heat shock protein 27 (HSP27) (Fig. 1B, C). Molecular chaperones such as HSP27 can defend against protein misfolding after sublethal stressful stimuli (4). Immunocytochemical experiments demonstrated intracellular localization of Prx1 (Fig. 1D), which increased 6 h after OGD treatment in the cytosol of endothelial cells (Fig. 1D, E).

Characterization of OGD-induced Prx1 ubiquitination in endothelial cells

Unexpectedly, our western blot data demonstrated a continual increase in the density of a broad, high-molecular-weight (>118 kDa) band for Prx1 starting 6 h after OGD treatment (Fig. 2A). A similar increase in a high-molecular-weight band (>118 kDa) was detected following OGD treatment after probing with an anti-ubiquitin antibody (Fig. 2B). The OGD-induced ubiquitination of Prx1 was confirmed and extended in HBMECs (Fig. 3 A, B) and mouse cerebral microvascular endothelial cells (bEnd.3) (Supplementary Fig. S2B).

Inhibition of proteosomal uptake with MG132 or lactacystin also increased the high-molecular-weight isoforms of Prx1 (Fig. 2C and Supplementary Fig. S3). Probing with an anti-Prx1 antibody in ubiquitin immunocomplexes from OGD-treated endothelial cells revealed a predominant band larger than 118 kDa (Fig. 2D and Fig. 3C). OGD-induced ubiquitination of Prx1 was confirmed by the immunoprecipitation of Prx1 followed by immunoblotting with an anti-ubiquitin antibody (Fig. 2E and Fig. 3D). Consistently, western blot analysis of cell extracts from OGD-treated cells demonstrated that high-molecular-weight conjugates of Prx1 were significantly reduced in *ubiquitin-K48R*-transfected endothelial cells (Fig. 2F and Fig. 3E, F).

The role of Prx1 during proapoptotic cascades after OGD treatment

Proapoptotic proteins were identified by immunoblotting of EA.hy926 cells transfected with either an empty vector or

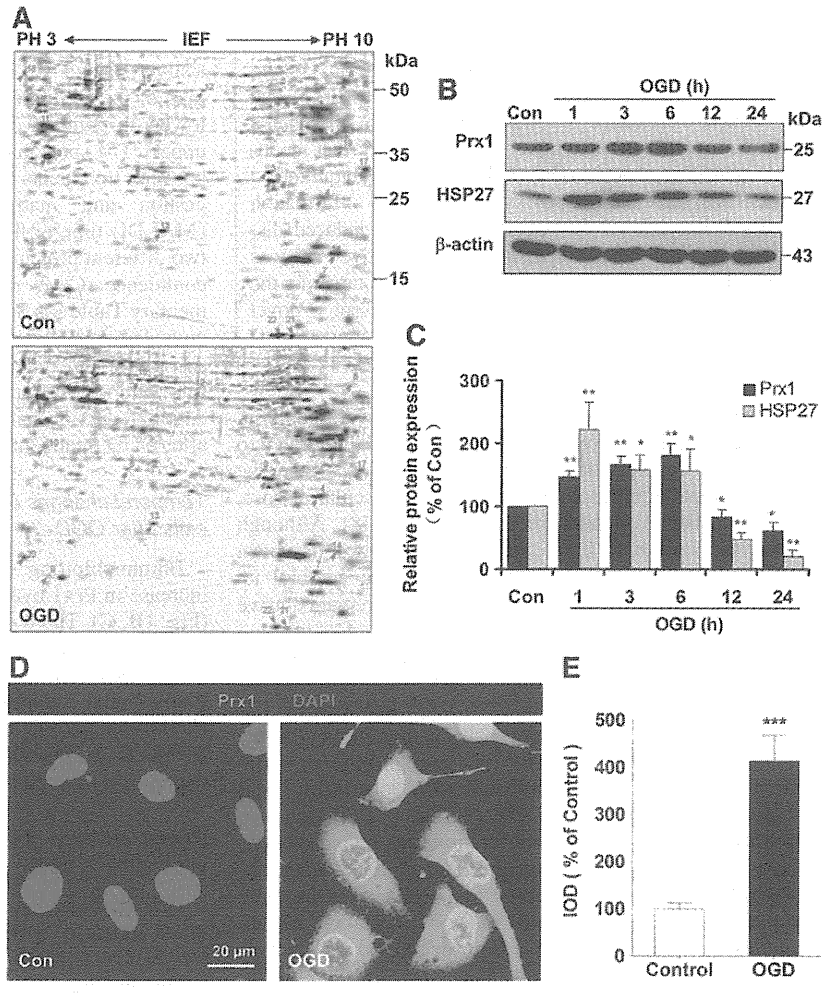

FIG. 1. The proteomic identification of differentially expressed proteins after OGD in endothelial cells. (**A**) Representative silver-stained two-dimensional gel of control and OGD-treated EA.hy926 endothelial cells. Whole proteins (450 μg) were separated on a non-linear pH gradient (3–10) followed by 12% SDS-PAGE. (**B**) Time course of Prx1 and HSP27 protein levels in cell lysates of endothelial cells following OGD. Quantifications of the temporal changes of Prx1 and HSP27 protein levels are shown in (**C**). Immunoblots are representative of three independent experiments. $*p<0.05$; $**p<0.01$ *versus* control. Immunoblotting with an anti-β-actin antibody showed equal amounts of loaded protein in each lane. (**D**) Changes in the immunostaining of Prx1 (green) 6 h after OGD. Subcellular localization of Prx1 was determined by laser confocal microscopy. Data are representative of three independent experiments. Scale bar = 20 μm. (**E**) Quantification of Prx1 immunofluorescence expressed as IOD as described in the Materials and Methods section. $***p<0.001$ *versus* control. IOD, integrated optical density; HSP27, heat shock protein 27; OGD, oxygen–glucose deprivation; Prx1, peroxiredoxin 1; SDS-PAGE, sodium dodecyl sulfate–polyacrylamide gel electrophoresis. To see this illustration in color, the reader is referred to the web version of this article at www.liebertpub.com/ars

a *Prx1* expression vector following OGD insult (Fig. 4). Calnexin is a type I integral endoplasmic reticulum (ER) membrane chaperone involved in folding newly synthesized (glycol) proteins (8). Overexpression of Prx1 significantly inhibited calnexin, PERK, and Ire-1α degradation (Fig. 4A, B) and also inhibited caspase-3 and poly ADP-ribose polymerase (PARP) cleavage (Fig. 4C, D). Exposure of vector-transfected cells to OGD for 6 h decreased the phosphorylation of anti-apoptotic proteins, such as phospho-ERK (Thr202/Tyr204) and phospho-FKHR (Ser256) (forkhead transcription factor Foxo1), and also decreased the protein levels of heme oxygenase-1 (HO-1) but increased the phosphorylation of c-Jun N-terminal kinase (JNK) and P38 (Fig. 4E, F). By contrast, overexpression of *Prx1* after OGD injury resulted in significant upregulation of anti-apoptotic proteins in endothelial cells (Fig. 4E, F). Exposure of vector-transfected cells to OGD for 6 h elevated terminal deoxynucleotidyl transferase dUTP nick end labeling (TUNEL)-positive staining (Fig. 4G, H), whereas overexpression of Prx1 effectively decreased TUNEL staining (Fig. 4G, H). The apoptosis of endothelial cells was determined using flow cytometry with Annexin V-FITC/propidium iodide (PI). In contrast to control cells (2.20%), we found that OGD treatment induced elevation in the fraction of Annexin V/PI-positive cells (49.92%). Moreover, *Prx1* small interfering RNA (siRNA) transduction further exaggerated OGD-induced cell death (Fig. 4I). The present data demonstrate that Prx1 elicits an anti-apoptotic effect after OGD injury in endothelial cells, coinciding with its antioxidant function in the endothelium (31).

E6AP activation contributes to Prx1 stress response after OGD

Since Prx1 has been identified as a novel E6AP-binding protein (33), the present study further elaborates the role of E6AP in ubiquitination of Prx1 during OGD. Representative blots are presented in Figure 5A and show that E6AP was activated following OGD exposure over 1–24 h (Fig. 5A). Similar change of E6AP was confirmed in HBMEC (Supplementary Fig. S4A, B) and bEnd.3 endothelial cells after OGD (Supplementary Fig. S2B). Immunocytochemical analysis of the endothelial cells revealed OGD-induced strong immunoreactivity for E6AP (red fluorescence) that was undetectable in control cells (Fig. 5B–D and Supplementary Fig. S4C, D), which suggests that OGD-induced ubiquitination of Prx1 is associated with E6AP activation.

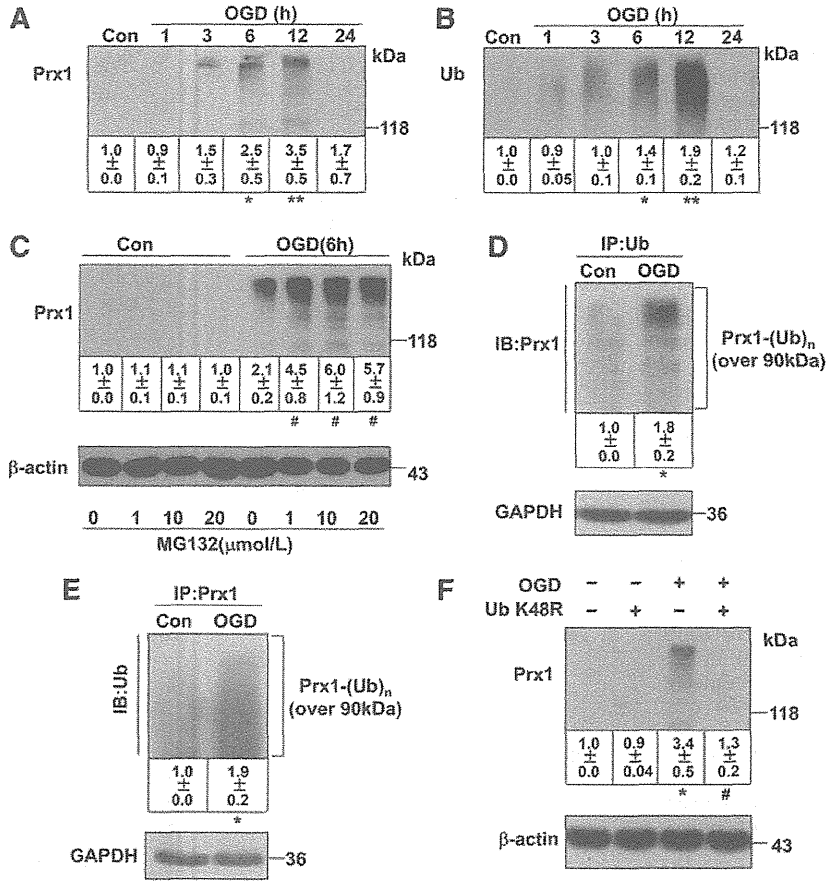

FIG. 2. OGD induces ubiquitination of Prx1 in EA.hy926 endothelial cells. (**A**) Temporal changes in the high-molecular-weight Prx1 isoform were observed in OGD-treated endothelial cells. The accumulated polyubiquitinylated proteins were detected by western blot analysis with anti-Prx1 antibody. (**B**) Protein ubiquitination status after OGD treatment in endothelial cells. The accumulated multiubiquitinylated proteins were detected by western blot analysis with an anti-ubiquitin antibody. (**C**) The changes in polyubiquitinated Prx1 were detected following OGD treatment of endothelial cells with or without proteasome inhibitors. The endothelial cells were treated with 1, 10, or 20 μM MG132 or DMSO 30 min before OGD. The cells were then washed, harvested after 6 h OGD, and analyzed for polyubiquitinated Prx1 levels. (**D**) The OGD-induced ubiquitination of Prx1 was detected by the immunoprecipitation of ubiquitin followed by immunoblotting with an anti-Prx1 antibody. (**E**) Immunoprecipitation of Prx1 from cell lysates of OGD-treated endothelial cells followed by blotting with an anti-ubiquitin antibody. (**F**) The ubiquitin K48R mutant decreased OGD-induced Prx1 ubiquitination in endothelial cells. Endothelial cells were cultured and transfected with plasmid DNA encoding the *ubiquitin-K48R* mutant or an empty plasmid, followed by OGD and immunobloting analysis. Immunoblots are representative of three independent experiments. Data are expressed as the percentage of values of control (mean ± SEM). $^{*}p < 0.05$; $^{**}p < 0.01$ *versus* control; $^{\#}p < 0.05$ *versus* OGD.

E6AP and the active-site cysteine-to-alanine-inactivated mutant E6AP were expressed in mammalian *p3869HA-E6AP C-A* cells (22, 46). Here, after 48 h of transfection, siRNA knockdown of *E6AP* (Fig. 5E, F) or transfection with the *E6AP C-A* mutant (Fig. 5G, H) both significantly blunted the ubiquitination of Prx1 in OGD-treated endothelial cells.

Nitrosative stress associated with the Prx1 defensive response after OGD

The $ONOO^-$ donor 3-morpholinosydnonimine (SIN-1) induced early dose-dependent elevation of Prx1 (Supplementary Fig. S5A, B) and Prx1 ubiquitination (Fig. 6A, B) in endothelial cells as detected by immunoblot, accompanied by increased Prx1 immunostaining (Fig. 6C) and activation of E6AP (Fig. 6D). Whereas increased nitrotyrosine immunostaining and E6AP immunoreactivity were observed in OGD-treated cells (Fig. 6E, F), inhibition of $ONOO^-$ with uric acid markedly reduced both nitrotyrosine and E6AP immunostaining after OGD exposure (Fig. 6E). This was confirmed by western blot (Fig. 6G, H). A similar result was observed in endothelial cells treated with $ONOO^-$ decomposition catalysts (FeTPPS, 1 μM) (Supplementary Fig. S6A, B). E6AP immunoprecipitates from the cell lysates were probed with anti-nitrotyrosine antibody (Fig. 6I). The results

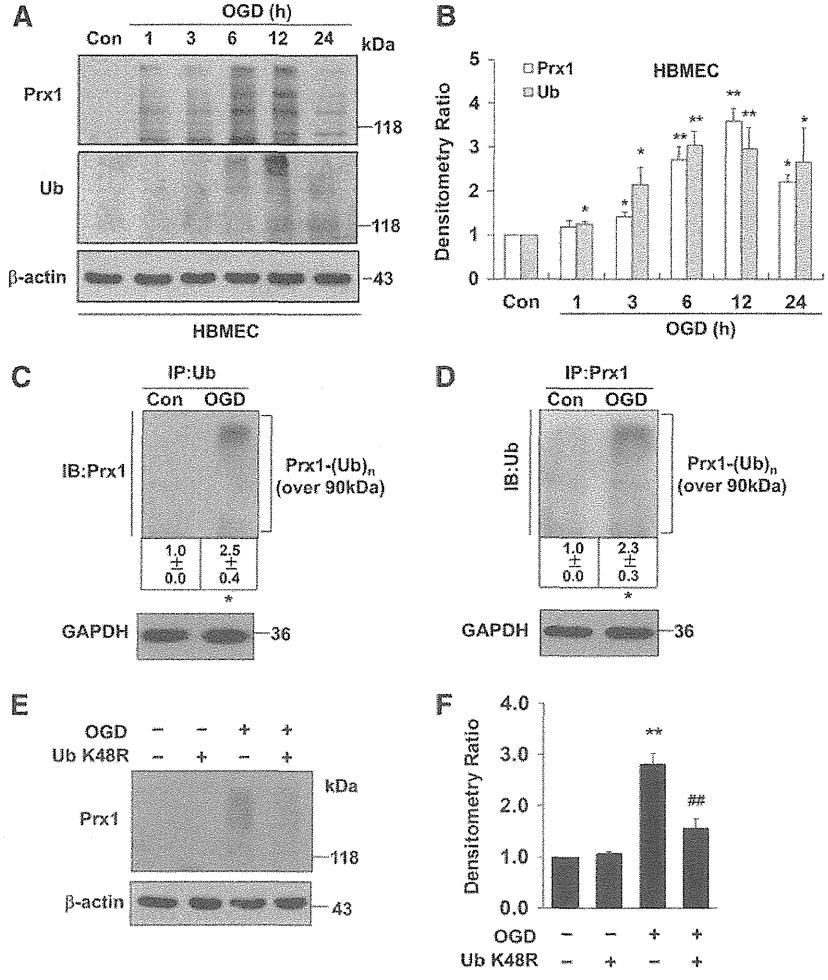

FIG. 3. The ubiquitination of Prx1 in OGD-treated HBMEC. (**A**) The time-dependent change of OGD-induced Prx1 and ubiquitin expression in HBMECs was detected by western blot. (**B**) Densitometry of the western blots for (**A**) was normalized by the level of β-actin as an internal control. (**C**) OGD-treated HBMEC endothelial cells were lysed and subjected to immunoprecipitation with antibodies to ubiquitin. The resultant precipitates were then subjected to immunoblot analysis with antibodies to Prx1. (**D**) Immunoprecipitation of Prx1 from lysed HBMEC with or without OGD treatment were collected for immunoblot analysis with ubiquitin antibody. (**E**) The *ubiquitin-K48R* mutant transfection attenuates Prx1 ubiquitination in OGD-treated endothelial cells. HBMEC were cultured and transfected with plasmid DNA encoding the *ubiquitin-K48R* mutant or an empty plasmid. (**F**) Densitometry of the western blots for (**E**) was normalized by the level of β-actin as an internal control. Immunoblots are representative of three independent experiments. Data are expressed as the percentage of values of control (mean ± SEM). $^{*}p < 0.05$; $^{**}p < 0.01$ *versus* control; $^{\#\#}p < 0.01$ *versus* OGD. HBMEC, human brain microvascular endothelial cell.

demonstrated that the E6AP/nitrotyrosine interaction in OGD-treated endothelial cells was significantly increased. Consistently, OGD-induced tyrosine nitration of E6AP was further confirmed by the immunoprecipitation of nitrotyrosine followed by immunoblotting with an anti-E6AP antibody (Fig. 6J). In addition, Prx1 immunoprecipitates from the lysates were probed with anti-nitrotyrosine antibody demonstrating that OGD did not induce Prx1 protein co-immunoprecipitate with nitrotyrosine (Supplementary Fig. S7). Melatonin blunted the ubiquitination of Prx1 in OGD-treated cells (Supplementary Fig. S8), suggesting that nitrosative stress induced Prx1 ubiquitination during OGD.

E6AP activation contributes to Prx1 stress response in brain microvessels after transient middle cerebral artery occlusion in mice

Since there are limited *in vivo* data on the degradation of Prx1 by ubiquitin ligases in ischemic brain, we used a mouse transient middle cerebral artery occlusion (tMCAO) model for further study. The immunoreactivity for E6AP was observed predominantly in the ipsilateral brain microvessel endothelium 6 h after tMCAO (Fig. 7A-e), accompanied by increased Prx1 immunoreactivity (Fig. 7A-d). A representative Z-stack image is shown in Figure 7B. However, after 24 h, Prx1 was downregulated where E6AP remained upregulated in the brain microvessel endothelium (Fig. 7A, g-i). Ubiquitination of Prx1 was elevated significantly in the brain microvessels 6 h after MCAO (Fig. 7C, D), whereas Prx1 staining was observed in microvessels of sham-operated animals where ubiquitin staining was absent. To further determine E6AP as a key modulator in nitrosative stress-mediated cerebrovascular damage *in vivo*, we stereotaxically delivered a lentivirus carrying mouse *shE6AP* into the ventricle in mice 2 weeks before MCAO, followed by ischemia and 24 h reperfusion. Western blot analysis showed that lentivirus-mediated cerebral *E6AP* knockdown reduced cerebrovascular damage, which was demonstrated by preventing ischemia-induced dephosphorylation of prosurvival kinases and tight junction proteins breakdown (Fig. 7E–G).

Lentiviral-Prx1 brain transduction protects against neurovascular damage in tMCAO mice

Two weeks after the cerebroventricular injection of a lentiviral-GFP vector encoding mouse *Prx1* (LV-*Prx1*), there was efficient and sustained GFP fluorescence in the brain ventricles (Fig. 8A), cortex (Fig. 8B), hippocampus, and

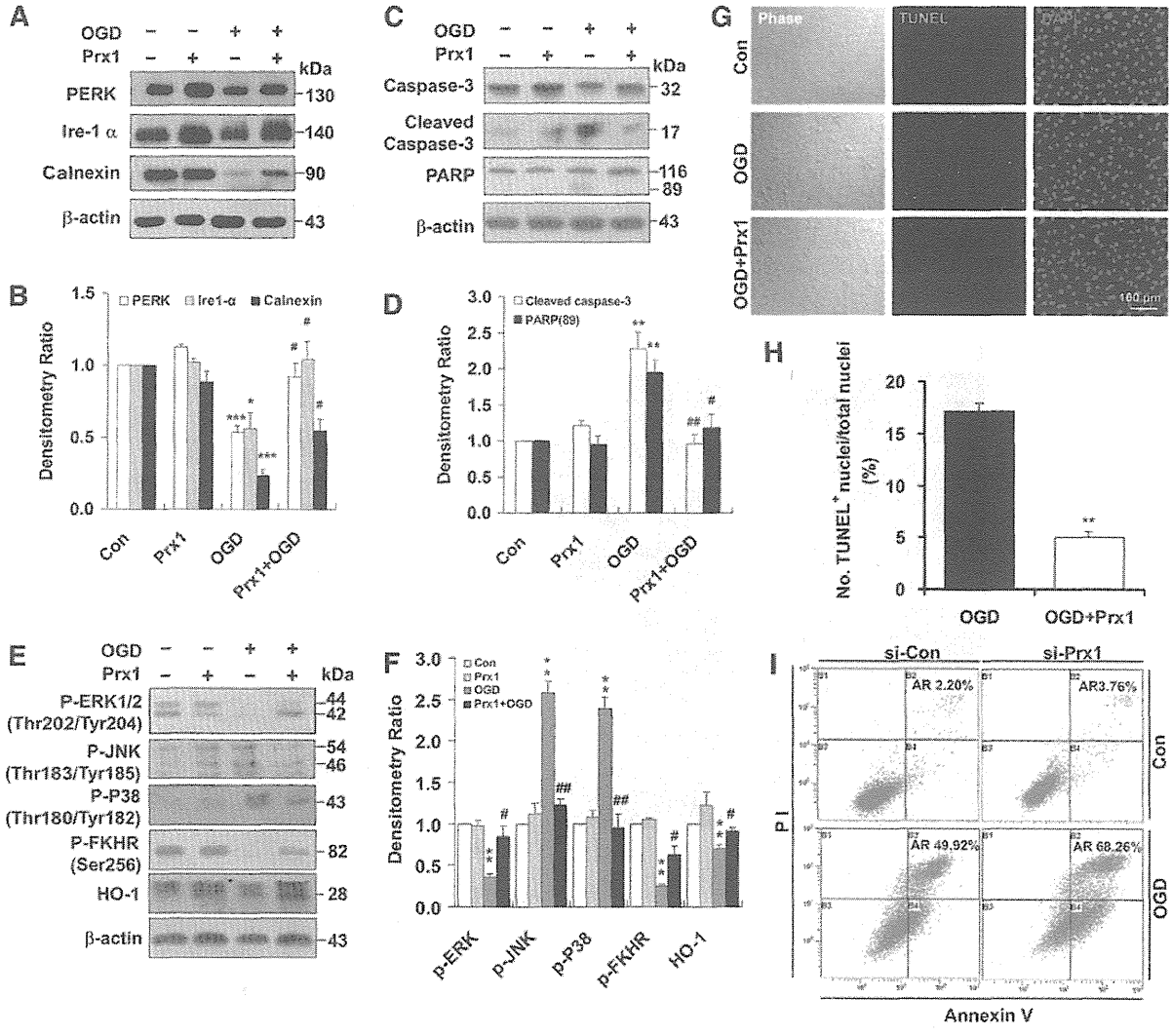

FIG. 4. Role of Prx1 in the OGD-induced apoptotic cascade in endothelial cells. (**A**) The effects of Prx1 on OGD-induced ER stress signaling were determined by immunoblotting. (**B**) Densitometry of western blots for PERK, Ire-1α, and calnexin levels 6 h after OGD, with or without *Prx1* transfection. Data are expressed as densitometry ratio of control (mean ± SEM). $^{*}p < 0.05$; $^{***}p < 0.001$ *versus* control; $^{\#}p < 0.05$ *versus* OGD. (**C**) The effects of Prx1 overexpression on OGD-induced caspase-3 and PARP levels were evaluated by immunoblotting. EA.hy926 cells were cultured and transfected with plasmid DNA encoding *Prx1* or an empty plasmid using Attractene. (**D**) The quantification data for blots are shown in (**C**). Data are expressed as densitometry ratio of control (mean ± SEM). $^{**}p < 0.01$ *versus* control; $^{\#}p < 0.05$; $^{\#\#}p < 0.01$ *versus* OGD. (**E**) The effects of Prx1 overexpression on OGD-induced protein levels were evaluated by immunoblotting. Cells were transfected with *Prx1* plasmid followed by 6 h of OGD or control stimulation. Cell lysates were prepared and resolved by SDS-PAGE. The proteins were immunoblotted with antibodies against phospho-ERK, phospho-JNK, phospho-P38, phospho-FKHR (Ser256), and HO-1. (**F**) Quantitative analysis of protein levels for (**E**) was performed by densitometry. Data are expressed as densitometry ratio of control (mean ± SEM). $^{**}p < 0.01$ *versus* control; $^{\#}p < 0.05$; $^{\#\#}p < 0.01$ *versus* OGD. (**G**) Changes in apoptosis 6 h after OGD were detected using the TUNEL assay. Double staining was performed for TUNEL (green) and DAPI (blue). The representative images show the increased percentage of TUNEL-positive apoptotic endothelial nuclei (green fluorescence) 6 h after OGD. Scale bar = 100 μm. (**H**) Quantification of TUNEL-positive apoptotic endothelial cells with or without *Prx1* transfection. Apoptosis was dramatically reduced following the overexpression of the *Prx1* gene in endothelial cells after OGD. $^{**}p < 0.01$ *versus* OGD group. (**I**) Representative flow cytometric dot plots of apoptotic cells after OGD with or without *Prx1*siRNA transfection. Cultured EA.hy926 cells were stimulated for 6 h with OGD with or without *Prx1*siRNA transfection. Cells were double-stained with Annexin-V and PI and analyzed by FACS. Immunoblots are representative of three independent experiments. β-Actin was used as the loading control. DAPI, 4′,6-diamidino-2-phenylindole; ER, endoplasmic reticulum; HO-1, heme oxygenase-1; JNK, c-Jun N-terminal kinase; PARP, poly ADP-ribose polymerase; siRNA, small interfering RNA; TUNEL, terminal deoxynucleotidyl transferase dUTP nick end labeling; PI, propidium iodide. To see this illustration in color, the reader is referred to the web version of this article at www.liebertpub.com/ars

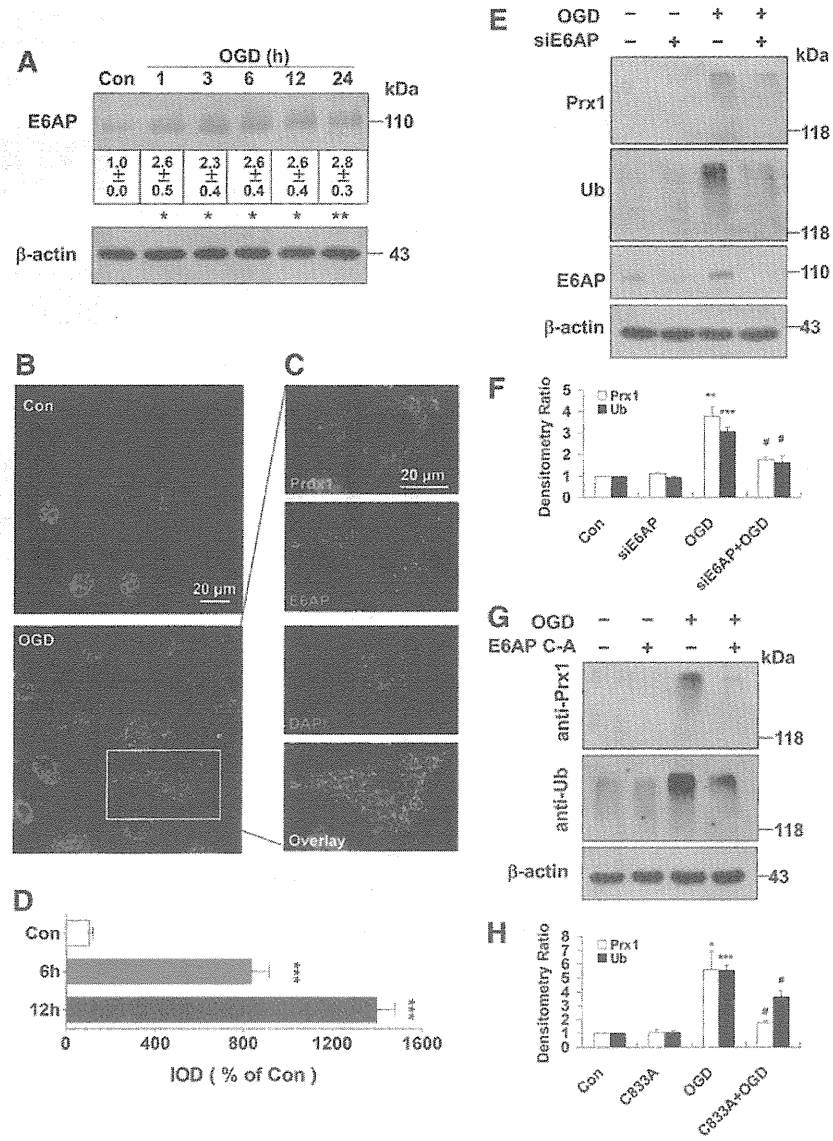

FIG. 5. E6AP activation contributes to the Prx1 stress response after OGD. (**A**) The representative image showing E6AP activation at the indicated time points after OGD treatment. Data are expressed as densitometry ratio of control (mean ± SEM). $*p < 0.05$; $**p < 0.01$ *versus* control. (**B**) Immunocytochemical analysis of E6AP expression after OGD treatment. Laser confocal microscopy demonstrated low to undetectable levels of E6AP in control cells. (**C**) Higher-magnification image of endothelial staining from the *insets* of (**B**). DAPI counterstaining indicates nuclear localization (blue). Scale bar = 20 μm. (**D**) Quantification of Prx1 immunofluorescence expressed as integrated optical density (IOD). $***p < 0.001$ *versus* control. (**E**) *E6AP* knockdown reduced the OGD-induced formation of multiubiquitinylated proteins. Cells were submitted to *E6AP* knockdown and OGD or the control condition for 6 h. Cell lysates were prepared and resolved by SDS-PAGE. The proteins were immunoblotted with antibodies against Prx1, E6AP, and ubiquitin. (**F**) Quantitative analyses for (**E**) are shown in the bar graph as densitometry ratio of control (mean ± SEM). $**p < 0.01$; $***p < 0.001$ *versus* control; $^{\#}p < 0.05$ *versus* OGD. (**G**) The $E6AP_{C\text{-}A}$ mutant decreased OGD-induced Prx1 ubiquitination in endothelial cells. EA.hy926 cells were cultured and transfected with plasmid DNA encoding the $E6AP_{C\text{-}A}$ mutant or an empty plasmid using Attractene. (**H**) Quantitative analysis of protein levels for (**G**) was performed by densitometry. Data are expressed as densitometry ratio of control (mean ± SEM). $*p < 0.05$; $***p < 0.001$ *versus* control; $^{\#}p < 0.05$ *versus* OGD. Immunodetection of β-actin was used as a loading control. Immunoblots are representative of three independent experiments. E6AP, E6-associated protein. To see this illustration in color, the reader is referred to the web version of this article at www.liebertpub.com/ars

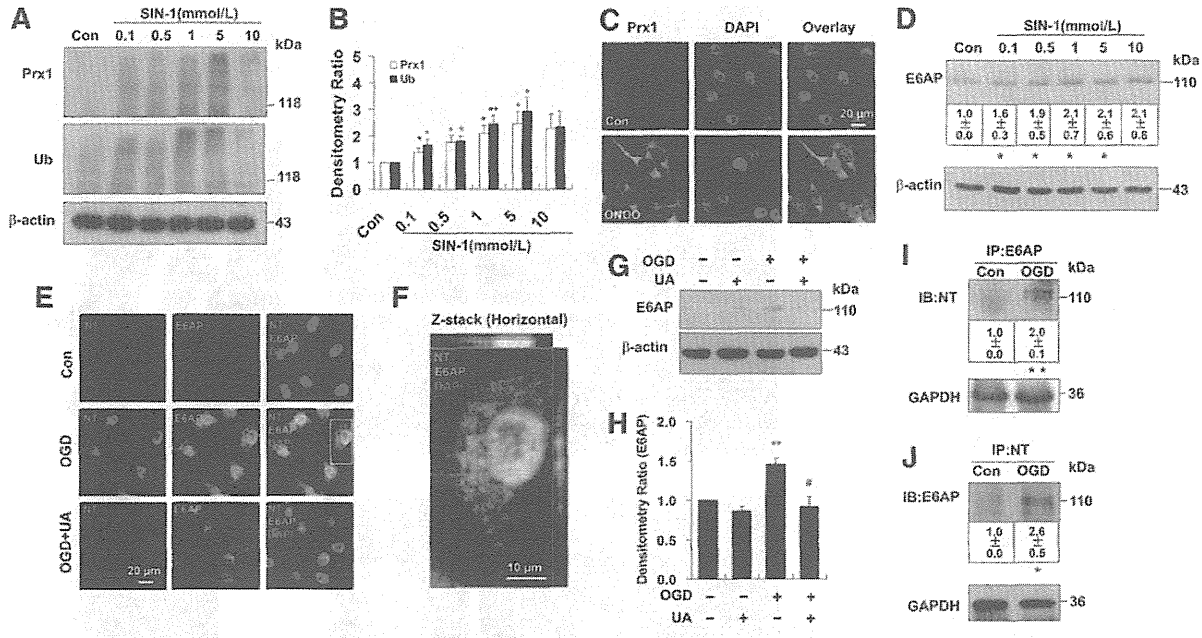

FIG. 6. Nitrosative stress is associated with ubiquitination of Prx1 in endothelial cells. (**A**) The ubiquitination of Prx1 after SIN-1 stimulation in endothelial cells. The blots were labeled with anti-Prx1 or anti-ubiquitin antibody and visualized with the ECL system. Molecular sizes are indicated on the *right*. (**B**) The SIN-1-induced changes in polyubiquitinated Prx1 were quantified and shown in the bar graph as densitometry ratio of control (mean ± SEM). $*p < 0.05$; $**p < 0.01$ *versus* control. (**C**) Immunocytochemical analysis of Prx1 level after $ONOO^-$ treatment by laser confocal microscopy. DAPI counterstaining indicates nuclear localization (blue). (**D**) The effects of SIN-1 treatment on E6AP protein levels were examined in cell lysates of endothelial cells. EA.hy926 endothelial cells were cultured with or without SIN-1 treatment for 6 h at the indicated concentrations. Immunoblots are representative of three independent experiments (mean ± SEM). $*p < 0.05$ *versus* control. (**E**) Fluorescence immunocytochemical staining of E6AP and nitrotyrosine 6 h after OGD in endothelial cells with or without 0.5 m*M* uric acid treatment. DAPI counterstaining indicates nuclear localization (blue). NT, nitrotyrosine; UA, uric acid. (**F**) Higher-magnification image of endothelial staining from the *insets* is shown in (**E**). (**G**) Effect of uric acid on E6AP expression in endothelial cells following OGD. Immunodetection of β-actin was used as a loading control. (**H**) Quantification of E6AP protein levels was performed using densitometric analysis of the immunoblots in (**G**). Immunoblots are representative of three independent experiments. Data are expressed as the percentage of values of control (mean ± SEM). $**p < 0.01$ *versus* control; $^{\#}p < 0.05$ *versus* OGD. (**I**) Immunoprecipitation of E6AP from cell lysates of OGD-treated endothelial cells followed by blotting with an anti-nitrotyrosine antibody. $**p < 0.01$ *versus* control. (**J**) The OGD-induced nitration of E6AP was detected by the immunoprecipitation of nitrotyrosine followed by immunoblotting with an anti-E6AP antibody. Immunoblots are representative of three independent experiments (mean ± SEM). $*p < 0.05$ *versus* control. SIN-1, 3-morpholinosydnonimine. To see this illustration in color, the reader is referred to the web version of this article at www.liebertpub.com/ars

striatum (Supplementary Figs. S9 and S10). Staining of brain sections from lentiviral-*GFP*-injected mice with a neuronal nuclear marker (NeuN) (Fig. 8B-d) and an endothelial marker CD31 (Fig. 8B-e, f) indicates that the vector successfully transduced cells in the brain. Although the lentiviral vectors might directly diffused into the brain parenchyma, the present data indicate that lentiviral vectors in cerebral ventricular can diffuse along the neurovascular scaffold. Immunohistochemical analysis of ipsilateral sections revealed stronger GFP fluorescence in tMCAO mice that formed a continuous interendothelial staining pattern that colocalized with CD31 (Fig. 8C, D).

The protective effects of Prx1 against ischemia-induced neurological and functional deficit were evaluated by the rotarod test and neurological score measurements. The neurological scores were decreased significantly, and rotarod time was increased in LV-*Prx1*-treated mice 24 h after tMCAO (Fig. 9A) and the infarct area was reduced accordingly (Fig. 9B). The breakdown products of spectrin and calcineurin were increased after tMCAO (Fig. 9C, D), coincident with BBB leakage (Fig. 9E, F). LV-*Prx1* treatment blocked the degradation of tight junction proteins zonula occludens-1 (ZO-1) and claudin5 (Fig. 9C, D, and G) and significantly reduced BBB leakage (Fig. 9E, F). LV-*Prx1* transduction reduced the $O_2^{\bullet -}$ level assessed from dihydroethidium staining in the penumbra region of mice 24 h after tMCAO (Fig. 9H, I).

Schematic illustration of the mechanisms by which nitrosative stress induces Prx1 ubiquitination during ischemic insult in endothelial cells

We hypothesize that ischemia-induced nitrosative stress causes an early increase in Prx1 production during the adaptive phase, whereas excessive or prolonged ischemia activates E6AP E3 ubiquitin ligase, which targets Prx1 for ubiquitination and degradation during the late phase, thereby degrading the Prx1-related antioxidant defense pathway and

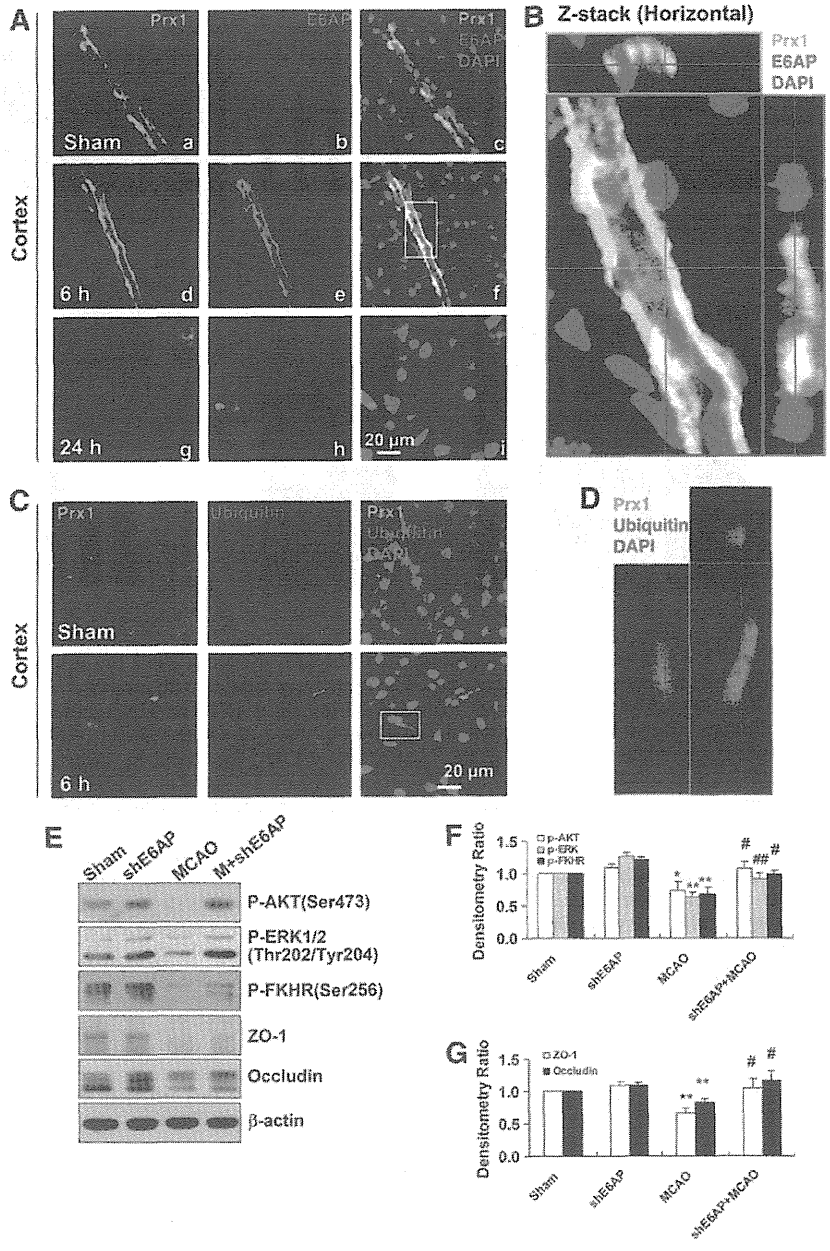

FIG. 7. E6AP activation is associated with Prx1 ubiquitination in brain microvessels of cerebral ischemia mice. (**A**) Double immunohistochemical staining for Prx1 and E6AP in the penumbra after tMCAO. Fluorescence staining for Prx1 (green) and E6AP (red) was performed in ipsilateral brain regions 6 and 24 h after brain ischemic injury in mice. (**B**) The orthogonal projections onto the $x-z$ (*upper*) and $y-z$ (*right*) planes are shown to confirm the colocalization of Prx1 and E6AP throughout the microvessels shown in (**A**). (**C**) Fluorescence immunohistochemical staining of Prx1 and ubiquitin in brain microvessels. Anti-ubiquitin (red) and Prx1 (green) staining was performed 6 h after tMCAO in mice. (**D**) Higher-magnification image of endothelial staining from the *insets* is shown in (**C**). Each image shown is representative of five independent mice. (**E**) The effect of *E6AP* knockdown on neurovascular damage after brain ischemia in mice. The lentivirus *E6AP* shRNA knockdown was used to silence *E6AP* mRNA. The protein extracts from penumbra brain region of mice were processed for western blotting to detect ZO-1, Occludin, and phosphorylated AKT, ERK, FHHR. (**F, G**) Quantitative analysis of protein levels in (**E**) was performed by densitometry. Densitometry values were normalized to the average of all sham values (mean ± SEM, $n=6$). $^{*}p<0.05$; $^{**}p<0.01$ *versus* sham mice; $^{\#}p<0.05$; $^{\#\#}p<0.01$ *versus* vehicle-treated mice. Immunoblotting with an anti-β-actin antibody demonstrated equal protein loading in each lane. tMCAO, transient middle cerebral artery occlusion; ZO-1, zonula occludens-1; shRNA, short hairpin RNA. To see this illustration in color, the reader is referred to the web version of this article at www.liebertpub.com/ars

rendering the endothelial cells in the microvessels susceptible to ischemic damage (Fig. 10).

Discussion

The present study demonstrates that in endothelial cells OGD treatment leads to oxidative and nitrosative stress that engage an early increase in Prx1 production and an antioxidant response. However, more prolonged or severe ischemia-mediated nitrosative stress ubiquitinates Prx1 by the activation of E6AP ligase, thereby degrading this antioxidant defense pathway. The translational studies in mice after MCAO demonstrated that neurovascular protection was coordinated by active Prx1.

Prx1 initiates the antioxidant response by scavenging free radicals formed in response to a diverse array of cellular stresses (40, 44). Upregulation of Prx1 may be secondary to the activation of NF-E2-related factor 2 (Nrf2) (24), as *Prx1* promoter has two antioxidant response elements that are putative binding sites for Nrf2. Indeed, we recently demonstrated that Nrf2 signaling coordinates the defense against ischemia/nitrosative stress in endothelial cells (49).

The ubiquitin–proteasome system is important for protein degradation in eukaryotic cells (19, 42). Unexpectedly, ubiquitin was not highly expressed in control endothelial cells, but high-molecular-weight Prx1-polyubiquitin ladders were observed after OGD or SIN-1 treatment. The aggregation of